STUDY OF MASS TRANSFER ACROSS HYDROFOILS FOR USE IN AERATING TURBINES

A THESIS
SUBMITTED TO THE FACULTY OF
UNIVERSITY OF MINNESOTA
BY

GARRETT MARK MONSON

IN PARTIAL FULFILLMENT OF THE REQUIREMENTS
FOR THE DEGREE OF
MASTER OF SCIENCE

DR. ROGER ARNDT
Substituting for JOHN S. GULLIVER

SEPTEMBER 2013

Acknowledgements

I would like to thank my advisors Dr. John Gulliver and Dr. Roger Arndt for their support and guidance. Dr. Gulliver has encouraged me to stretch beyond my previous experience and grow in new areas of civil engineering. Without Dr. Gulliver's advice and encouragement, this research would have been much more difficult. Many thanks go to Dr. Gulliver for being a model of academic and personal integrity. A special thanks to Dr. Arndt for filling in and helping to wrap up my research as Dr. Gulliver had to step back due to medical leave. The experience, wisdom, and support of my advisors has been invaluable.

I would also like to acknowledge Ellison Kawakami and Dr. Seung-Jae Lee for teaching me the ropes of the water tunnel and introducing me to the world of experimental fluid mechanics through trial by fire. Ellison has been essential in the success of my graduate work. The SAFL staff, especially Ben Erickson and Aaron Ketchmark, was an integral part in the completion of my work through their efforts to keep the water tunnel running throughout a lab renovation.

I am very grateful for the Hydro Research Foundation for funding my education and providing invaluable opportunity for learning and networking in the hydro power industry. Funding for the research was provided by The University of Minnesota, The Department of Energy, and Alstom.

I need to thank my family and friends. Your unending love and support has encouraged me to persevere and achieve my goals. A very special thank you goes to my parents for providing the opportunity for a great education from grade school through graduate work. My friends have provided perspective, insight, and comic relief. My wife, Kayla, has been and continues to be my inspiration and most valued support. I cannot express enough my gratitude enough to all who have shaped my academic career and my personal life. I am truly grateful.

Dedication

I dedicate this work to my wife Kayla. You awaken my spirit and inspire me to chase my dreams. Thank you for your love and support. I love you.

Abstract

Hydroelectric projects often have a low tailwater dissolved oxygen (DO) concentration. Low DO levels negatively impact the biota of the water body and are often regulated. Auto-Vented Turbines (AVTs) are one form of DO mitigation that is typically successful and cost-effective. Saint Anthony Falls Laboratory (SAFL) at the University of Minnesota (UMN) is partnering with the Department of Energy (DoE) and Alstom Engineering to conduct research developing a conventional hydropower turbine aeration test-bed for computational routines and a software tool for predicting the DO uptake of AVTs. The focus of this thesis is on the development of the test-bed through the conduct of physical experiments focused on measuring mass transfer across bubbles in various flow conditions. This test-bed will be a valuable database for verification of numerical models of DO uptake. Numerical models can simulate the parameters of the water tunnel and experimental set-up, then verify their accuracy by simulating the air entrainment rate, bubble size and mass transfer of the test-bed. The findings presented herein can lead to further optimization of AVTs, as well as reduce cost and regulatory uncertainty prior to hydropower relicensing or development.

Table of Contents

List of Tables

List of Figures

Chapter 1: Introduction

Background

A low dissolved oxygen (DO) concentration is one of the most cited water quality parameters downstream of hydroelectric dams. Dissolved oxygen is an indicator of stream health as it is essential for amphibious species such as fish, clams, invertebrates, etc [1]. Low DO can occur when reservoirs behind a dam become thermally stratified during warm summer months resulting in two zones of the reservoir that do not easily mix: (i) the warmer, upper epilimnion and (ii) colder, lower hypolimnion. The epilimnion usually has healthy DO concentrations due to its interaction with the atmosphere at the water's surface; whereas spring rains wash organic material into the hypolimnion where it depletes DO concentrations, sometimes to anoxic conditions. Intakes for hydro-electric turbines are often in this lower region and discharge cold waters with low DO concentrations downstream. To maintain their license to operate, hydroelectric projects must meet EPA requirements downstream, including minimum DO concentrations, and mitigation is therefore necessary.

There are several techniques available for mitigation of low DO, but one that has widespread interest throughout the hydropower industry is the use of auto vented turbines (AVTs). Auto vented turbines take advantage of naturally occurring sub-atmospheric pressures occurring within the turbine and vent air to these location through strategically placed ports and diffusers. They require no additional power consumption, as they utilize pressure differences to drive air flow. Auto vented turbines have been shown to effectively raise DO levels while the new runner design can often improve turbine efficiency and power output [2].

Literature Review

In the late 1980's the TVA started an initiative to develop physical modeling and numerical modeling tools for auto-venting turbine design and to demonstrate auto-venting turbine technology with a full-scale installation. Working together with Voith Hydro, Inc. and American Hydro let to the study and development of a new auto-venting runner for the Norris Dam site in Tennessee. Several venting options were evaluated including air injection through: a redesigned turbine hub, or deflector; discharge edges of the turbine blades; coaxial diffuser; discharge ring; draft tube cone; and combination of these. The locations of these options are shown in figure 1.

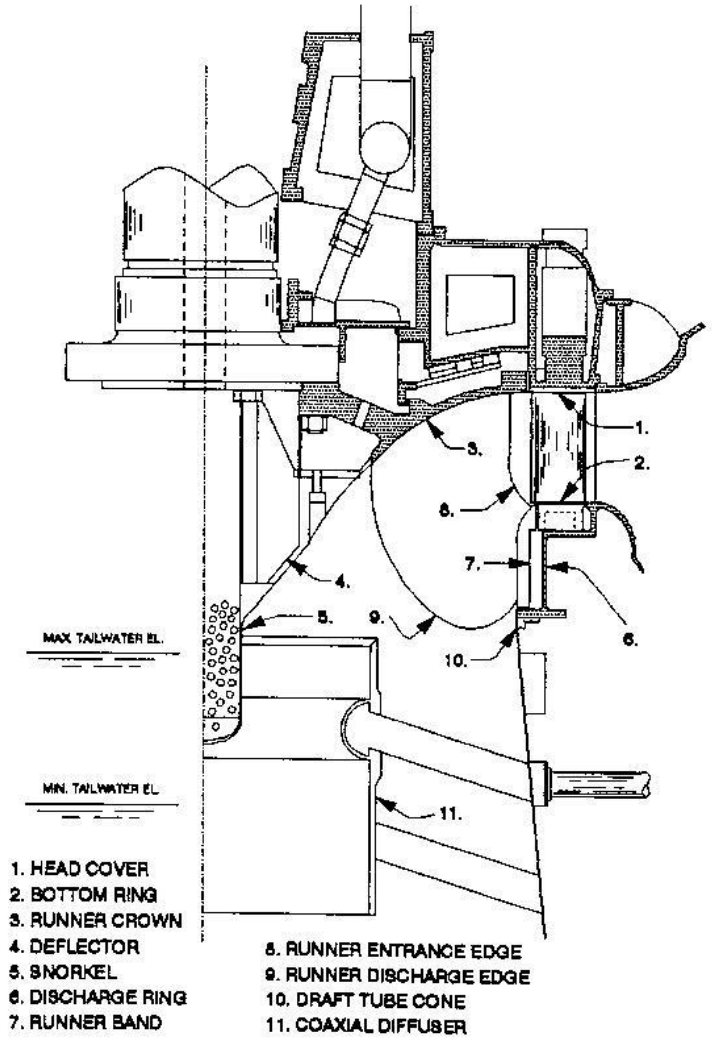

Figure 1. Several alternatives for turbine aeration [2]

In the early 1990's, physical model studies, of a new runner design showed an increase in capacity of 7 percent and efficiency of 1.8 percent when not aerating. While aerating, the results showed increased efficiency while operating with the discharge edges presumable due to reduced flow separation at high head/high gate conditions. The discharge ring, draft tube cone, and combination of discharge edge and draft tube cone provided a reasonable balance between efficiency losses and aeration performance. The largest efficiency losses were observed with the

coaxial diffuser [2]. These results are shown in figures 2 and 3. Efficiency loss is associated with the percent by volume of air to water flowing through the turbine as shown in figure 4.

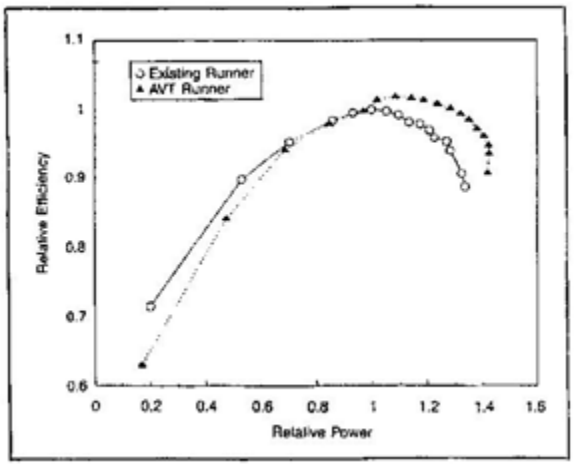

Figure 2. Efficiency results without aeration from model tests at Norris Dam [2]

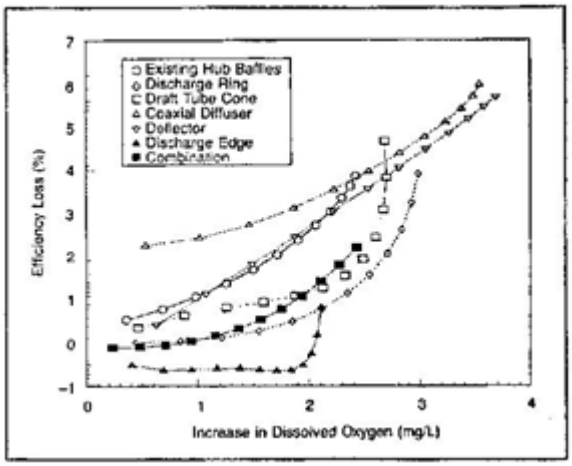

Figure 3. Typical efficiency loss and aeration results from model tests for a net head o 190 feet and maximum gate opening [2]

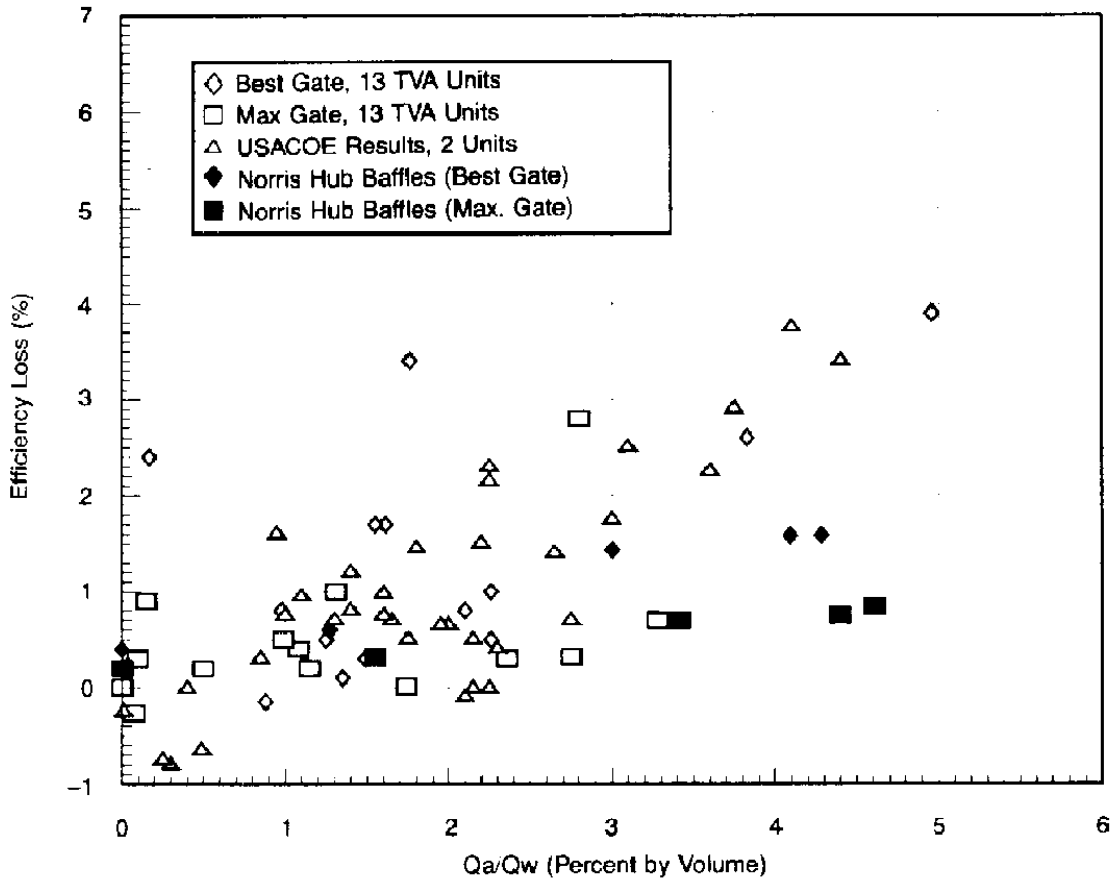

Figure 4. Measured losses in power generating efficiency during turbine aeration with a variety of techniques for 15 hydro units at eight TVA plants and one Corps of Engineers plant [2]

Following the model studies, full scale auto-vented turbine runners were installed at Norris Dam in Tennessee. Using a variety of aeration techniques, an average DO level of 5.5 mg/L was obtained during low DO flows as shown in figure 5. This is near the target level of 6 mg/L.

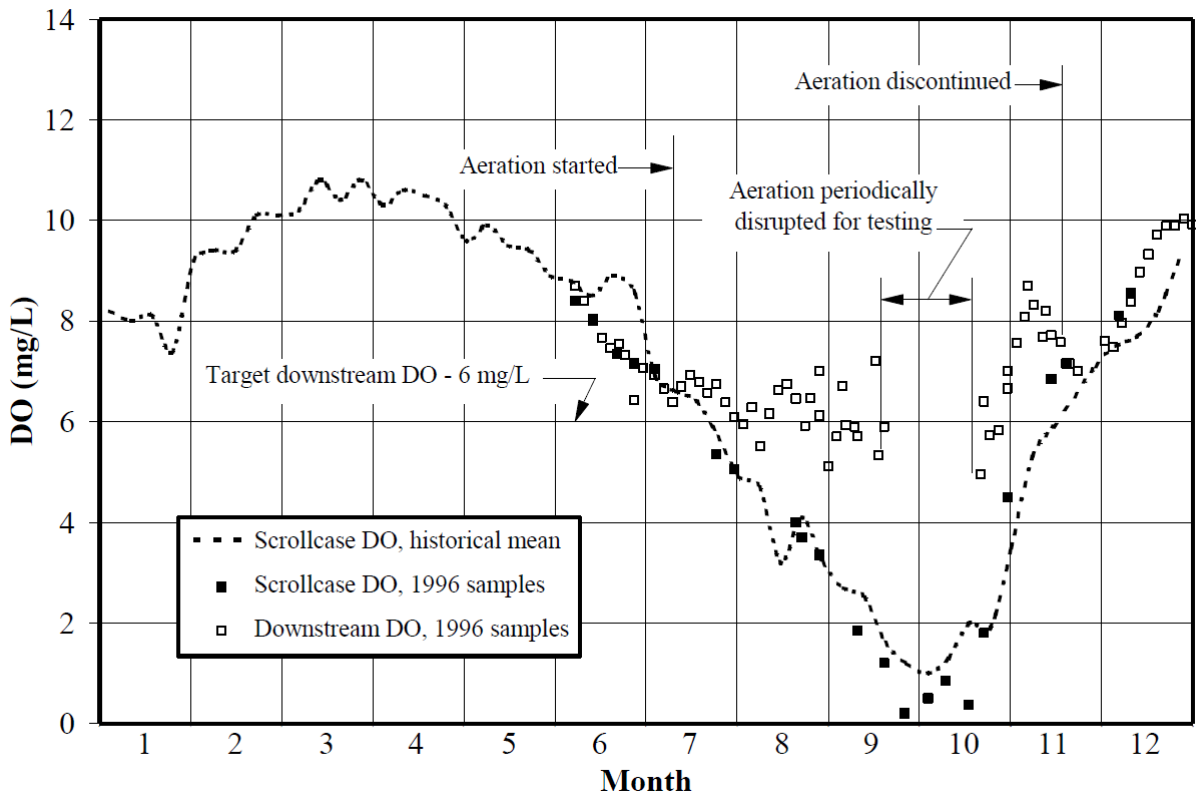

Figure 5. Dissolved oxygen improvement for Norris Dam, 1997 [3]

Auto vented turbines are an exciting technology, but require more investigation. Like most water resource technologies, AVTs are designed uniquely for each site. This can be an expensive process of rendering physical models to test the proposed design. Numerical models can be used in the design process to avoid rendering physical models, but there are a limited number of models focused on predicting DO uptake of AVTs. Research must be done to close the gap from a numerical flow field in a turbine to predicted DO uptake to improve the design of AVTs.

Project Approach

St. Anthony Falls Laboratory (SAFL) at the University of Minnesota (UMN) is developing a conventional hydropower turbine aeration test-bed for computational routines and software tool for Advanced Hydropower Development in Subtopic 3.1: Environmental Mitigation

Technologies for Conventional Hydropower, System and Component Model Development. SAFL and the UMN are partnered with Alstom, a global leader in energy technology development and power generation to conduct and explore further avenues of AVTs. This research and development initiative is occurring in two coordinated efforts with extensive collaboration among each of the research teams.

Experimental data designed to be used as an effective verification of the software will be collected in the SAFL High Speed water tunnel. A hydrofoil, with a specially modified NACA 0015 profile designed for aeration studies, will be used. The bubbly wake generated by precisely metered ventilation flow will be measured. Bubble location and size distribution information will be captured using high speed photography and particle shadow velocimetry. These data will provide an extensive and rich dataset accessible for computational validation studies of the impact of entrained air upon the flow field, and the impact of the flow field upon air entrainment. There are three processes that are very important to the success of an aerating turbine: 1) for a given flow field, what will be the quantity of air that is entrained, 2) what will be the bubble size of the entrained air at a given location after entrainment and 3) what will the oxygen transfer be across these bubbles? All three of these processes will comprise the focus of the experiments, which will be completed using the NACA-0015 hydrofoil. A series of air injection experiments will be completed at several hydrodynamic conditions, allowing for quantitative analysis of aeration statistics and capabilities for the turbine blade hydrofoil designs. This experimental study will compliment numerical studies carried out by others in the ;program.

Through the research program described above, SAFL and Alstom will develop a powerful tool for advancing the development and implementation of aerating turbines at U.S. hydropower facilities. In addition, the experimental results will comprise an aeration test-bed for all manufacturers, increasing the reach of the U.S. DOE's efforts. The advanced aeration design capabilities resulting from utilizing this software will reduce the cost and regulatory uncertainty

prior to hydropower development. The adverse environmental impacts resulting from the low tailrace dissolved oxygen common to hydropower facilities will ultimately be reduced. Through improved environmental performance and decreased environmental impacts, this research effort will advance the capabilities and reduce the cost of energy resulting from conventional hydropower technologies. [4]

The focus of this thesis is on physical experiments being conducted for this research. Exploratory experiments have been conducted to establish the methodology for creating the test-bed and study the impact of varying water velocity, airflow, and angle of attack (AoA) on mass transfer and resulting DO uptake.

Chapter 2: Facilities

The St. Anthony Falls Laboratory (SAFL) at the University of Minnesota (UMN) is uniquely equipped to address the research needs for developing a conventional hydropower turbine aeration test-bed. The SAFL High Speed Water Tunnel, seen in figure 6, and degassing loop allow for efficient and accurate testing of aeration experiments.

SAFL High Speed Water Tunnel

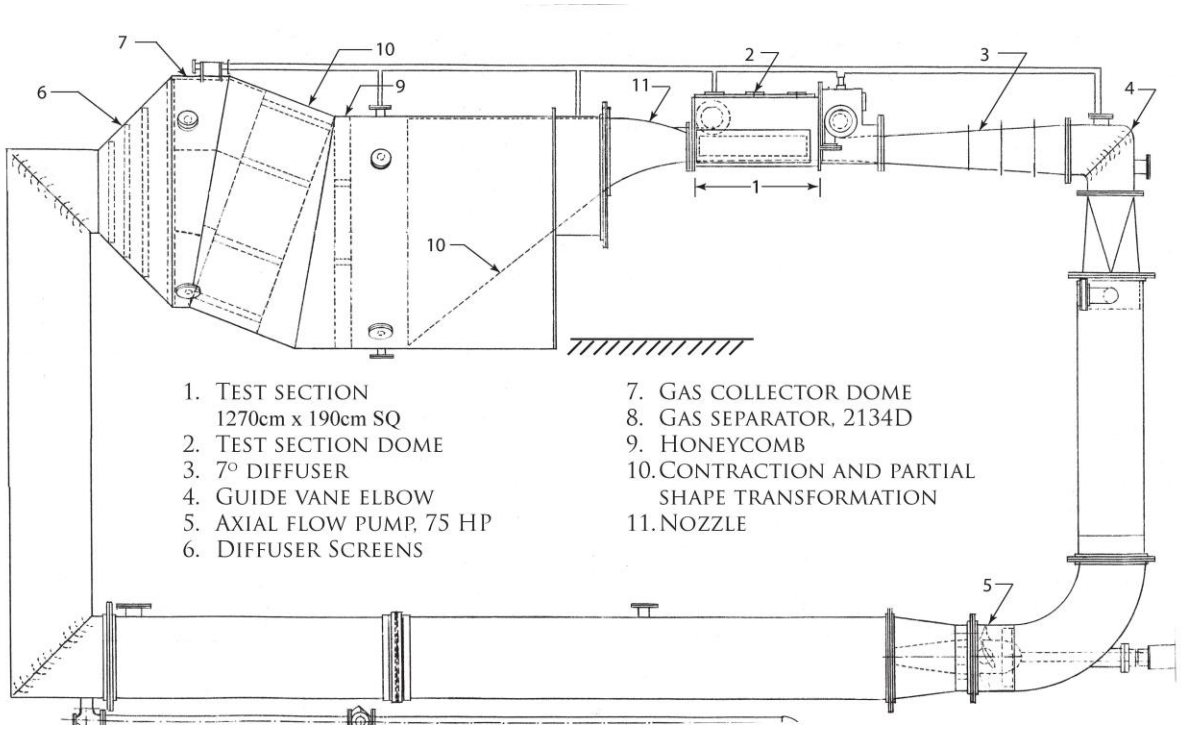

Figure 6. SAFL High Speed Water Tunnel

The SAFL High Speed Water Tunnel is a recirculating, closed-jet facility with absolute pressure regulation. The total volume of the tunnel is approximately 17.8 m^3. It is capable of velocities in excess of 20 m/s in the test section. The test section measures 0.19 m (W) x 0.19 m (H) x 1.27 m (L). It is instrumented with pressure taps and provides optical access from 3 sides. Test section windows can be fitted with interchangeable mounting plugs to install instrumented hydrofoils, lift and drag force balances and scale models. The water tunnel is powered by a modern 75HP Alternating Current Motor. Available experimental tools include digital strobe photography, digital video, high resolution Stereo Time-Resolved Particle Image Velocimetry (TR-PIV), high resolution Time-Resolved Particle Shadow Velocimetry (TR-PSV), 2-component Laser Doppler Velocimetry (LDV) with automated traversing system, Phase Doppler Anemometry (PDA) for particle/bubble sizing, and now Shadow Image Velocimetry (SIV).

The water tunnel is specially designed to remove large quantities of air that may be injected in the test section during experiments. This allows extended ventilation experiments to be conducted without recirculating bubbles. In its current configuration the tunnel features a closed test section with a thin Mylar roof between the test section and a tank that may be instrumented with hydrophones. The measured uniformity of the flow is better than 1% and the turbulence level is found to be approximately 0.3%. [5]

Degassing Loop

A degassing loop was developed and constructed at SAFL to strip dissolved gasses from the water in the high speed water tunnel. Water is withdrawn from the bottom of the tunnel upstream of the test section and pumped up to a degassing chamber with a diameter of 0.45 meters and a height of 4.8 meters for a chamber volume of approximately 0.76 m^3. The water is discharged into the chamber through eight randomly oriented nozzles, creating a cloud of droplets falling through the chamber. Dissolved gasses are stripped from these droplets by applying a vacuum pressure as low as half an atmosphere. This vacuum pressure is created by the free-jet water tunnel at SAFL which uses gravity fed river water through a contraction causing a venturi affect to create a vacuum pressure which is translated to the nearby degassing chamber via a pipe. When the droplets have passed through the chamber, they collect at the bottom and are conveyed by gravity through a pipe to the high speed water tunnel just upstream of the motor.

The degassing loop was created to improve the degassing capabilities of the high speed water tunnel at SAFL. This system reduces the amount of time taken to degas the high speed water tunnel between aeration experiments. The dissolved oxygen (DO) concentrations can now be reduced to an acceptable starting concentration of approximately 4 ppm from super saturated concentrations in excess of 8 ppm in less than 24 hours, as opposed to previous methods which

took three days to effectively lower DO concentrations prior to experiments. The degassing loop can also be utilized to change cavitation water quality conditions for study of cavitation inception.

NACA-0015 Ventilated Hydrofoil

The NACA-0015 is a symmetrical hydrofoil with a thickness to chord ratio of 15%. The span and chord length are 19 cm and 81 mm respectively. The hydrofoil is ventilated through the body to a slit on the suction side of the leading edge as seen in Figure 7. Two air supply lines through the hydrofoil ensure even distribution of the air as seen in Figure 8.

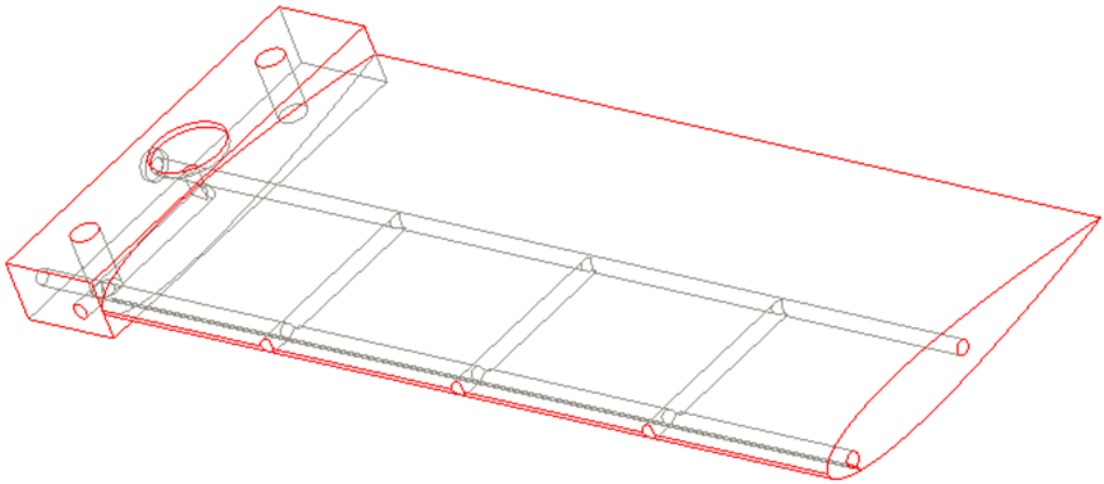

Figure 7. CAD drawing of ventilated NACA-0015

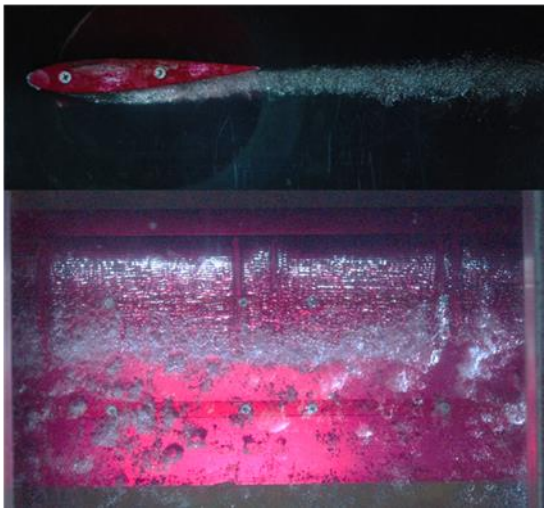

Figure 8. Distributed bubbly wake of NACA-0015

Chapter 3: Measurements

The SAFL High Speed Water Tunnel is instrumented with pressure transducers, thermistor, mass flow controller, DO measurement, and high speed imaging capabilities. This instrumentation is controlled by two computers, one with LabView software for analog data collection, and one with LaVision software for high speed image capture. The instrumentation is described below.

Pressure

Figure 9. Valedyne pressure transducer

Valedyne pressure transducers are used to measure absolute pressure in the test section and in the elbow vane downstream of the diffuser in the SAFL High Speed Water Tunnel, as well as differential pressure between the settling chamber and test section. Due to the large volume of the settling chamber and its surface being at atmospheric pressure, it is assumed to have a negligible velocity. Differential pressure measurement is then used to calculate test section velocity. Uncertainties in velocity are discussed in Appendix B.

Temperature

Figure 10. Yellow Springs stainless steel thermistor

A Yellow Springs 2252 Ohm stainless steel thermistor is used to monitor water temperature in degrees Celsius in the SAFL High Speed Water Tunnel. The thermistor is mounted in a plug on the settling chamber where it is submerged in the circulating flow of the water tunnel.

Mass Flow

Figure 11. Omega Mass Flow Controller

An FMA-2609A Omega mass flow controller is used to set and measure air flow to the model in the test section from a compressed air line. The mass flow is controlled via an analog set point. This analog signal is sent as a command voltage from the LabView software on the

controlling PC and corresponds to an airflow rate in standard liters per minute (SLPM). The FMA-2609A Series mass flow controller uses the principle of differential pressure within a laminar flow field to determine and control mass flow rate. A laminar flow element (LFE) inside the meter forces the gas into laminar (streamlined) flow. Inside this region, the Poiseuille equation dictates that the volumetric flow rate be linearly related to the pressure drop. A differential pressure sensor is used to measure the pressure drop along a fixed distance of the LFE. This, along with the viscosity of the gas, is used to accurately determine the volumetric flow rate. Separate absolute temperature and pressure sensors are incorporated and correct the volumetric flow rate to SLPM. An electronic valve is adjusted to match the determined flow rate to the set flow rate. The process is iterated until the desired flow rate is obtained. [6]

Dissolved Oxygen

Figure 12. Hach LDO probe and controller

Hach luminescent dissolved oxygen (LDO) probes and controller are used to measure DO concentration in both the settling chamber and the elbow vane downstream of the diffuser of the SAFL High Speed Water Tunnel. LDO probes are quickly becoming a popular alternative to

Clark cell DO probes based on their non-consumptive technology, minimum maintenance, and high level of accuracy. [7]

Imaging

Figure 13. Photron APX-RS High Speed Camera

A Photron APX-RS High Speed Camera is used to capture images for characterizing the bubbles in the bubbly wake of a ventilated hydrofoil. The camera is capable of 3000 fps at full resolution and is controlled by DaVis high speed imaging software made by LaVision.

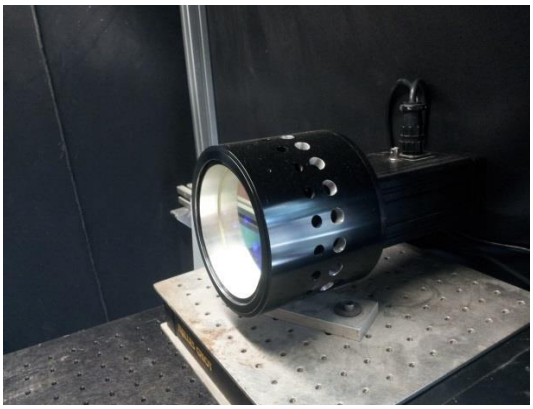

Figure 14. Custom ISSI pulsed LED array

An Integrated Silicon Solution Inc. custom made pulsed LED array is used to backlight the bubbles in the imaging process. The LM4XP is a 4-inch air-cooled LED based light source. The array of 20 LED's is driven beyond spec to increase the light output to 3 Watts, however, the

duty cycle is restricted to 5%. The operation of the LM4XP is controlled by setting the voltage to an external BNC on the lamp housing and the rise and fall time is less than 500-ns.

Chapter 4: Experiments

Experimental Setup

The SAFL High Speed Water Tunnel is instrumented with the devices discussed in Chapter 3 in the following manner:

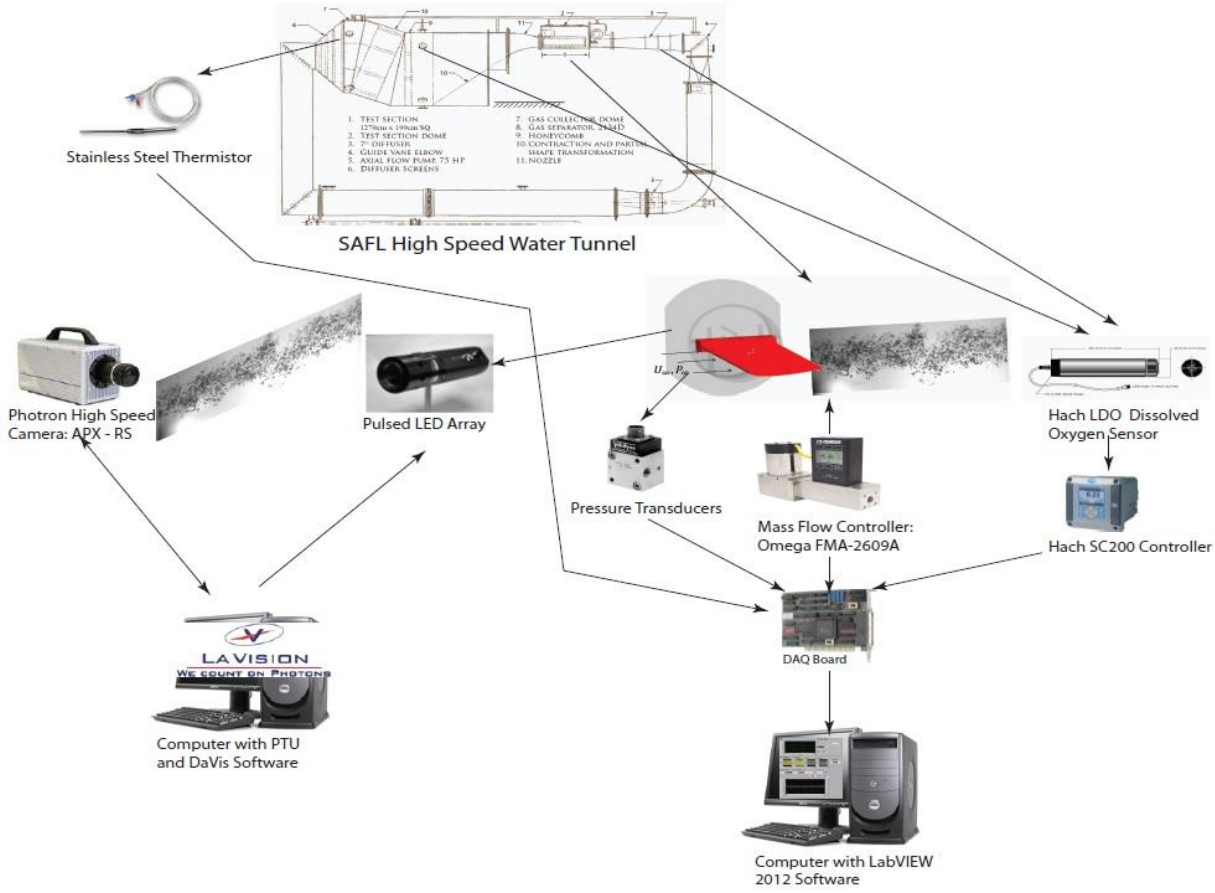

Figure 15. Experimental Setup

This experimental setup utilizes two computers. One computer running LabView12 software interfaces with the sample and hold data acquisition board, allowing for truly

simultaneous capture of the data across all channels. This computer records the data from all instrumentation involving physical measurements. The second computer runs LaVision's Davis 7.2 high speed imaging software and interfaces with the high speed camera and pulsed LED array to image the bubbly wake.

The experimental plan was set up to capture a range of velocities and airflow rates to cover various void ratios and turbulent conditions. Based on the capacities of the SAFL High Speed Water Tunnel and other instrumentation, the following experimental plan was compiled:

Table 1. Experimental Plan

AoA (0°, -4° ,or -8°)	Qa (SLM)		
U (m/s)	10	20	30
10	β		β
7.5		β	
5	β		β

Angles of attack of -8, -4, and 0 degrees were studied with varying test section free stream velocities and mass flow rates. Table 1 can then be filled in with the resulting β values found by fitting experimental results to the one-dimensional model discussed in Chapter 5.

Methodology

For a given experiment, the angle of attack is set by rotating the plug which the ventilated hydrofoil was mounted on. The angle of attack was measured using a digital protractor. With the angle of attack set, the tunnel is calibrated for pressure measurements and resulting velocity as outlined in Appendix D. After calibration, the degassing loop is run to reduce the DO concentration to approximately 4 ppm. This starting value was chosen to ensure that a large enough change in DO concentration is captured during experiments and that the degassing time is still short enough to allow for efficient use of the facilities. Degassing loop operation is outlined in Appendix B.

Once the starting value is reached, the degassing loop is stopped and the water tunnel is run at approximately 8 m/s until the water is thoroughly mixed to smooth out the spatial variation in DO concentration and temperature. The water is now prepped for an experiment. To begin the experiment, the test section velocity is set at the desired speed, the LabView12 software is commanded to begin recording, and the airflow rate is set. The experiment is left to run for 10 hours before it is stopped and the whole process is started again for the next condition.

To conduct imaging, the water in the water tunnel need not be degassed. The desired angle of attack, test section velocity, and airflow rate can be set to replicate the conditions of the full mass transfer experiment. The imaging of the bubbly wake can then be executed using the DaVis 7.2 software on the LaVision computer.

Chapter 5: One-Dimensional Model

Theories Applied

A one-dimensional model of the change in dissolved oxygen (DO) concentration in the SAFL High Speed Water Tunnel was developed to fit the physical experiments to known mass transfer theory with a single coefficient. The theory of Azbel's k_L (equation 1) [8] and simplified conservation equations (equation 2) [9] are the basis of this model.

Equation 1: $$k_L \approx \frac{D^{1/2}}{4\pi} \frac{U^{3/4}}{(lv_f)^{1/4}} \frac{(1-\varphi)^{1/2}}{(1-\varphi^{5/3})^{1/4}}$$

Where: D = diffusivity

v_f = kinematic viscosity

l = characteristic length scale

U = characteristic velocity

φ = void fraction

Equation 2: $$U\frac{dC}{dx^*} = k_L\alpha(C^*-C)$$

Where: C = DO concentration

C^* = function of pressure and saturation concentration

x^* = moving coordinate system, $x^* = x-ut$

α = ratio of bubble surface area to measurement volume of water

$=(4\pi r^2 * N)/V_w$

Where: r=Sauter Mean Diameter/2

N=number of bubbles in section $(\varphi * \frac{V_w}{V_b})$

V_w=volume of water in current section of tunnel

V_b=volume of bubble with Sauter Mean Diamter

Equation 1 assumes that Azbel's k_L can be set equal to the right hand side of his equation by multiplying by some constant β. This β becomes the coefficient that is fit to match the experimental data. Other theories such as Boyle's Law, Ideal Gas Law, and Continuity are used to compute the change in bubble size and the velocities throughout the water tunnel.

Model Application

The model breaks down the water tunnel into six sections: test section, diffuser, right leg, bottom leg, left leg, and settling chamber. The model requires inputs of test section velocity, test section pressure, average bubble diameter, airflow rate, water temperature, initial DO concentration, and DO saturation concentration. The model begins in the test section where it calculates Azbel's k_L based on the inputs and tunnel geometry. Next, a fourth order Runge Kutta method is executed to solve for the change in DO in the water in the stream wise direction. The average bubble diameter is adjusted based on the change in bubble diameter caused by mass transfer and pressure changes using the Ideal Gas Law. The model then steps to the next section where it executes the same procedure using the new DO concentration from the previous tunnel section. This process is completed in a loop around the tunnel until reaching the settling chamber. After calculations in the settling chamber are completed, any bubbles that have not been consumed by mass transfer are assumed to leave the tunnel via the gas collector dome. The loss

of bubbles in the settling chamber was verified by visually observing the flow from the settling chamber into the test section. No bubbles were observed. The loop is then repeated with the new concentration in the settling chamber as the initial concentration in the test section. The loop is repeated until a steady state concentration is approached.

The time it takes for the water to complete one loop is known based on calculated velocities throughout water tunnel. This time is used to plot the calculated DO concentrations in areas of the tunnel where Hach LDO probes are located as a function of time.

Chapter 6: Discussion and Results

Aeration experiments were conducted in the water tunnel at various angles of attack and void ratios per the experimental plan laid out in Chapter 4. The experimental results were then fit with the one-dimensional model discussed in Chapter 5. The inputs for each condition were put into the model and then the appropriate saturation concentration was input to fit the steady state concentration and the β coefficient was adjusted to fit the curvature of the experimental data. These results can be seen in Appendix A. Due to hardware failure, bubble imaging was delayed and an Sauter Mean Diameter of 0.41 mm from the case of a ventilated wake at angle of attack of -8 degrees and a free stream test section velocity of 7 m/s was applied across all conditions. The bubble characteristics from this conditions are shown below in figure 16 and figure 17.

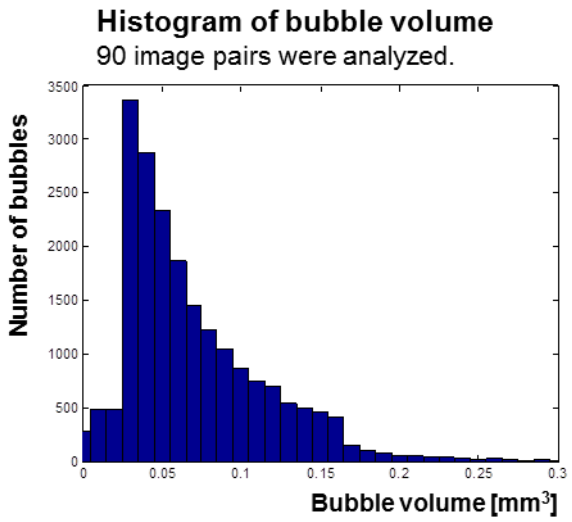

Figure 16. Distribution of bubble size for entire data set.

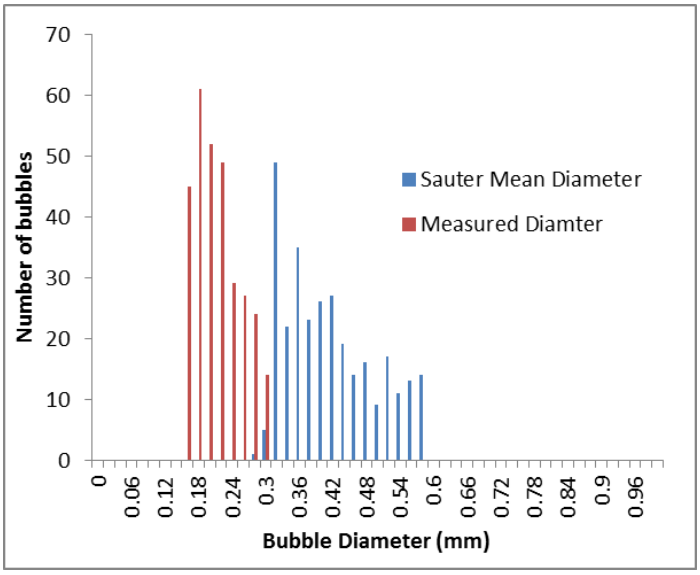

Figure 17. Sauter Mean Diameter and measured diameter from sample image.

The assumed bubble size needs to be addressed in future research. Fitting the experimental data to the one-dimensional model yielded the results shown in Tables 2 through 5.

Table 2. β coefficients for AoA -8 degrees

AoA -8°	Qa (SLM)		
U (m/s)	10	20	30
10	0.28		0.33
7.5		0.27	
5	0.3		0.25

Table 3. β coefficients for AoA -4 degrees

AoA -4°	Qa (SLM)		
U (m/s)	10	20	30
10	0.4		0.31
7.5		0.3	
5	0.27		0.25

Table 4. β coefficients for AoA 0 degrees

AoA 0°	Qa (SLM)		
U (m/s)	10	20	30
10	0.38		0.32
7.5		0.31	
5	0.28		0.24

Table 5. Summary of results

AoA	U (m/s)	Qw (m^3/s)	Qa (SLPM)	Qa (m^3/s)	Measured ϕ	ϕ at std. conditions	β
-8	5	0.181	10	0.00019	0.00106	0.0554	0.3
-8	5	0.181	30	0.00057	0.00317	0.1662	0.25
-8	7.5	0.271	20	0.00047	0.00174	0.0739	0.27
-8	10	0.361	10	0.00033	0.00091	0.0277	0.28
-8	10	0.361	30	0.00102	0.00283	0.0831	0.33
-4	5	0.181	10	0.00019	0.00106	0.0554	0.27
-4	5	0.181	30	0.00056	0.00309	0.1662	0.25
-4	7.5	0.271	20	0.00046	0.00172	0.0739	0.3
-4	10	0.361	10	0.00036	0.00100	0.0277	0.4
-4	10	0.361	30	0.00103	0.00286	0.0831	0.31
0	5	0.181	10	0.00020	0.00110	0.0554	0.28
0	5	0.181	30	0.00056	0.00312	0.1662	0.24
0	7.5	0.271	20	0.00050	0.00184	0.0739	0.31
0	10	0.361	10	0.00036	0.00099	0.0277	0.38
0	10	0.361	30	0.00103	0.00285	0.0831	0.32

The β coefficients found by fitting the experimental data to the one-dimensional model show a range across all conditions of 0.24 to 0.4 with a mean of 0.30 and a standard deviation of 0.04 as shown in Table 6.

Table 6. β coefficient statistics

Angle of Attack	Mean β	Std. Dev.
-8 degrees	0.29	0.03
-4 degrees	0.31	0.05
0 degrees	0.31	0.05
All Conditions	0.30	0.04

By plotting the β coefficients as a function of measured void ratio (Figure 18), a clear trend occurs. There is a clear grouping of β coefficients across all angles of attack at similar conditions. From this information one can conclude that angle of attack is not a large factor in mass transfer in these experiments. It can be stated that angle of attack and resulting turbulent length scale have a negligible effect on mass transfer.

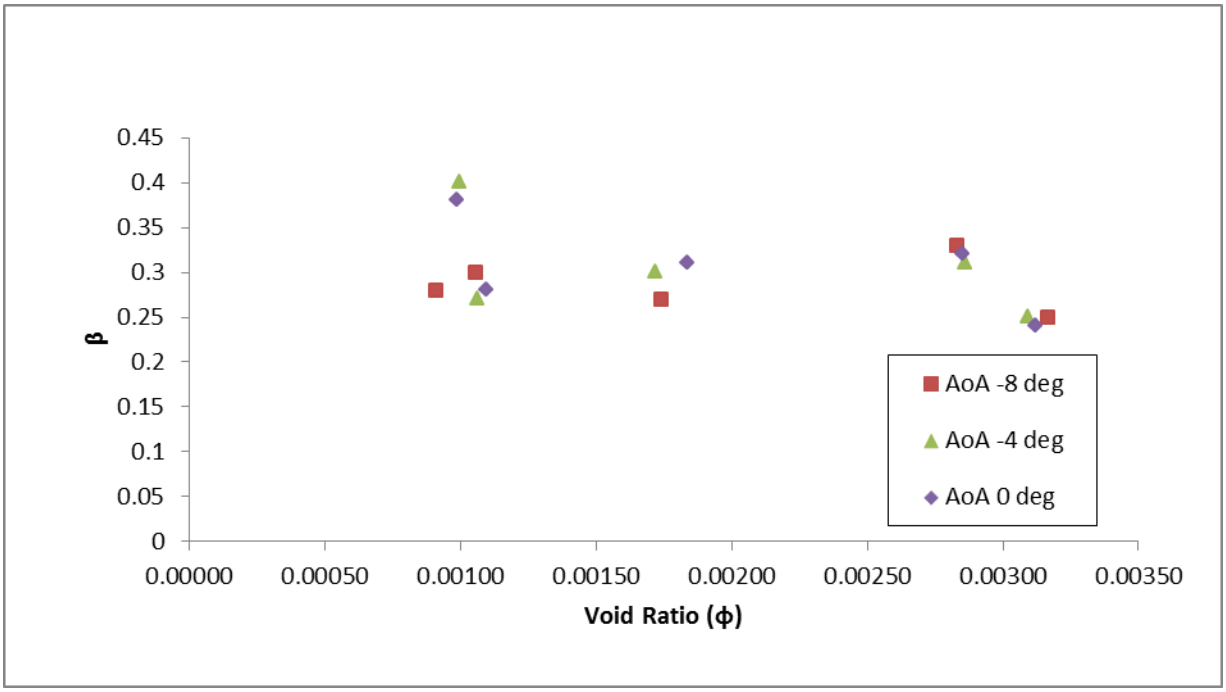

Figure 18. β coefficient vs. Measured Void Ratio

Plotting β coefficient as a function of test section velocity (Figure 19) and airflow (Figure 20) both show little correlation. This is some verification of the models, where the dependency upon characteristic velocity and void ratio is incorporated. There does appear to be a slight increase in β as velocity increases and void ratio decreases. This may be due to the ability of more turbulent flow to shear bubbles to a smaller diameter (better for mass transfer) at a lower void ratio. Future characterization of bubble characteristics across these conditions may also lead to more conclusive trends, based on the impact of bubble size in mass transfer.

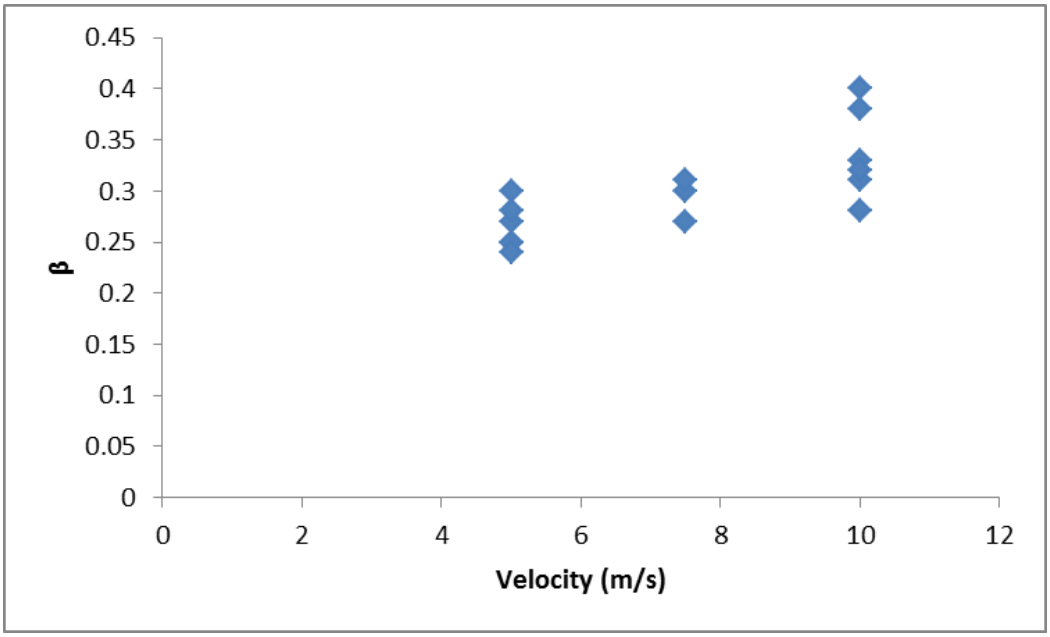

Figure 19. β coefficient vs. Test Section Velocity

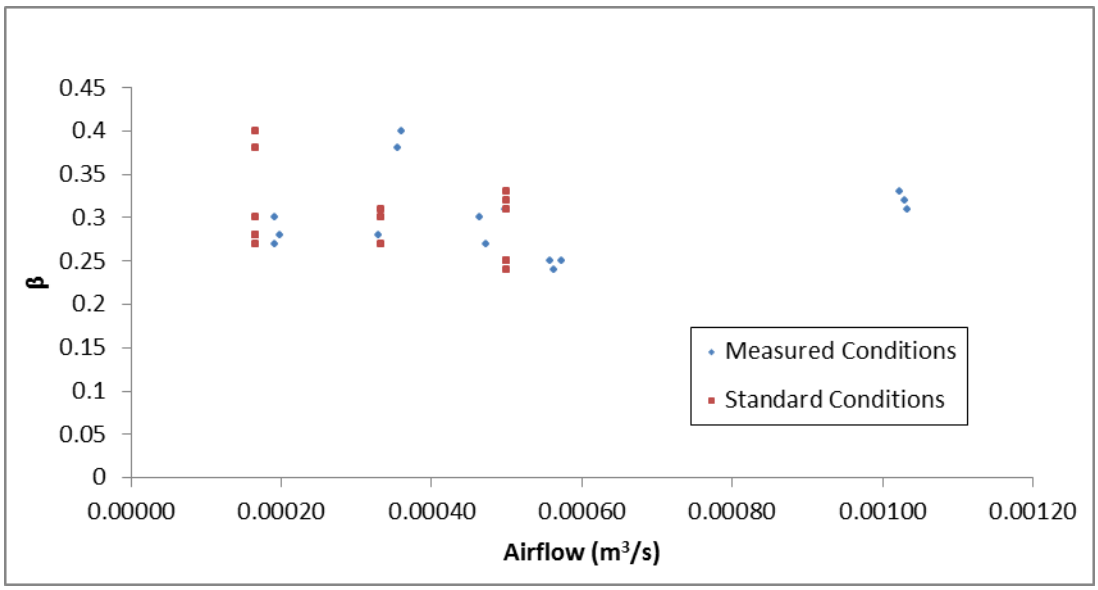

Figure 20. β coefficient vs. Airflow

If β is assumed to be a constant 0.3, the model can then be run and fit to experimental results by adjusting only the DO saturation concentration. This results in an imperfect fit of the model to the data in tems of the speed with which saturation is reached. This disparity is

highlighted below in figure 21. The worst case (poorest fit) of U = 10 m/s, Qa = 10 SLPM, and AoA = -4° with calculated β = 0.4 is displayed. The difference in time taken to reach saturation is approximately 75 minutes.

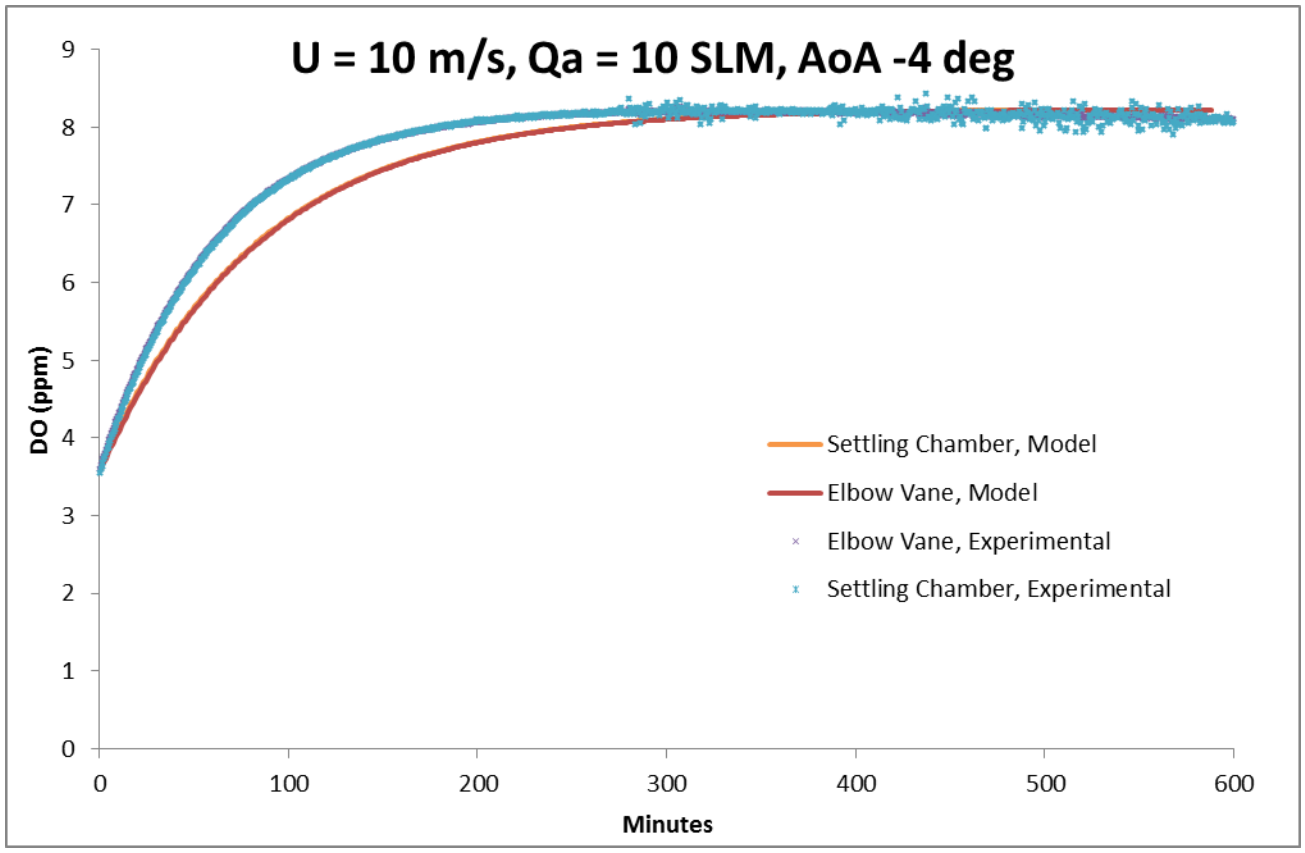

Figure 21. Disparity of time to saturation assuming β to be constant at 0.3

Based on the results of these experiments, additional experiments are recommended to complete bubble imaging to determine the impact of bubble characteristics upon mass transfer for these cases.

Chapter 7: Summary

Conclusions

Hydroelectric power is one of the most reliable renewable energies available. One adverse effect of hydroelectric dams is the discharge of water downstream with low dissolved

oxygen (DO) concentrations. To maintain their license or be approved for development, hydroelectric projects must mitigate these low DO concentrations to meet EPA standards. A form of mitigation that is gaining popularity are Auto Vented Turbines (AVTs). Auto Vented Turbines show the ability to mitigate low DO levels while maintaining efficient operation of the hydroelectric unit. [2] These AVTs are effective, but their designs are site specific and more exploration into their development is needed.

The St. Anthony Falls Laboratory (SAFL) at the University of Minnesota (UMN) is partnering with the Department of Energy (DoE) and Alstom Engineering to develop a conventional hydropower computational test-bed and software tool for the improvement of Auto Vented Turbines. As part of developing this test-bed, physical aeration experiments were conducted in the SAFL High Speed Water Tunnel to study the impact of various flow conditions on mass transfer across bubbles. A one-dimensional model was developed to lend insight into the mass transfer characteristics observed in these experiments.

A β coefficient to be used with Azbel's k_L value was studied and found to have an average value of 0.3 +/- 0.01 ($p = 0.95$) across the conditions of all experiments. This coefficient was not found to be highly correlated with the measured parameters in the experiments conducted. Additional experiments are recommended which will focus on bubble characteristics. Initial findings are promising of the ability to numerically relate dissolved oxygen to flow conditions occurring in AVTs. This is based on the minimal variation of the β coefficient and its ability to relate measured mass transfer to Azbel's theory.

Future Work

Research up to this pointed has focused on the establishment of a conventional hydropower computational test-bed including the instrumentation and development of experimental facilities and procedures needed to develop this test-bed. Unavoidable delays,

equipment failure, and need for improvement of instrumentation and facilities in addition to the refurbishment of the laboratory caused narrowing of the scope of work for this thesis. Future work should focus on measuring turbulence and bubble characteristics and relating these characteristics to flow conditions and previously attained mass transfer data. Specific focus should be on bubble diameter and it's relation to turbulent length scales and intensity. This can be achieved by implementing the SIV technique available at SAFL. More data on bubble characteristics and their relation to flow conditions is essential to linking DO uptake across bubbles to flow conditions.

Future collaboration with Alstom will study the impact of air injection strategy on DO uptake. Care should be taken to document bubble size and turbulence characteristics to be compared with the cases studied in this thesis. Based on the highly variable pressure profile around a hydrofoil, injection location may have a large impact on entrainment efficiency. It will also be interesting to observe the impact of differing injection locations on the ability to reduce cavitation, or improve flow field efficiency (runner efficiency in the field), both of which are major concerns in the hydropower industry.

Works Cited

[1] E. J. Thompson and J. S. Gulliver, "Wxygen Transfer Similitude for Vented Hydroturbine," *Journal of Hydraulic Engineering,* vol. 123, no. 6, pp. 528-538, 1997.

[2] P. A. March, T. A. Brice, M. H. Mobley and J. M. Cybularz, "Turbines for Solving the DO Dilema," *Hydro Review,* vol. 11, p. 1992, March 1992.

[3] P. Hopping, March P., T. Brice and J. Cybularz, *Update on Development of Auto-Venting Turbine Technology,* Norris, TN: Tennessee Valley Authority, 1997.

[4] J. Gulliver, R. Arndt and F. Sotiropoulos, "Turbine aeration design software for mitigation adverse environmental impacts resulting from conventional hydropower turbines," St. Anthony Falls Laboratory, Minneapolis, 2011.

[5] "SAFL High Speed Water Tunnel," University of Minnesota, 1 November 2011. [Online]. Available: http://cav.safl.umn.edu/facilities.htm.

[6] "Mass Flow Controllers," Omega, 2013. [Online]. Available: http://www.omega.com/pptst/FMA2600_FVL2600.html.

[7] D. T. O. Mitchell, "Luminescence Based Measurement of Dissolved Osygen in Natural Waters," Hach Company, Loveland, CO, 2006.

[8] D. Azbel, *Two-phase flows in chemical engineering,* K. Philip, Ed., New York, New York: Cambridge, 1981, p. 195.

[9] J. P. Giovannettone and J. S. Gulliver, *Gas Transfer and Liquid Dispersion Inside a Deep Airlift Reactor,* 4 ed., vol. 54, AIChE Journal, 2008, pp. 850-861.

Appendix A: Experimental Results: DO data used to compute β values

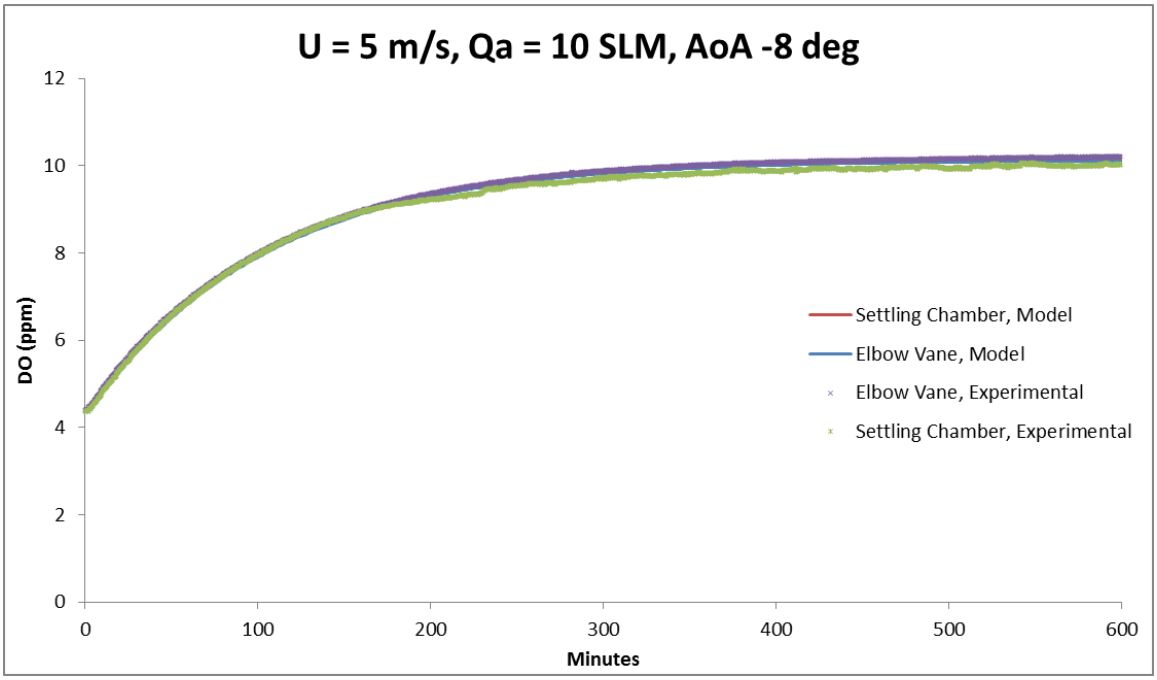
U = 5 m/s, Qa = 10 SLM, AoA -8 deg
DO (ppm)
Minutes
0
2
4
6
8
10
12
0
100
200
300
400
500
600
Settling Chamber, Model
Elbow Vane, Model
Elbow Vane, Experimental
Settling Chamber, Experimental

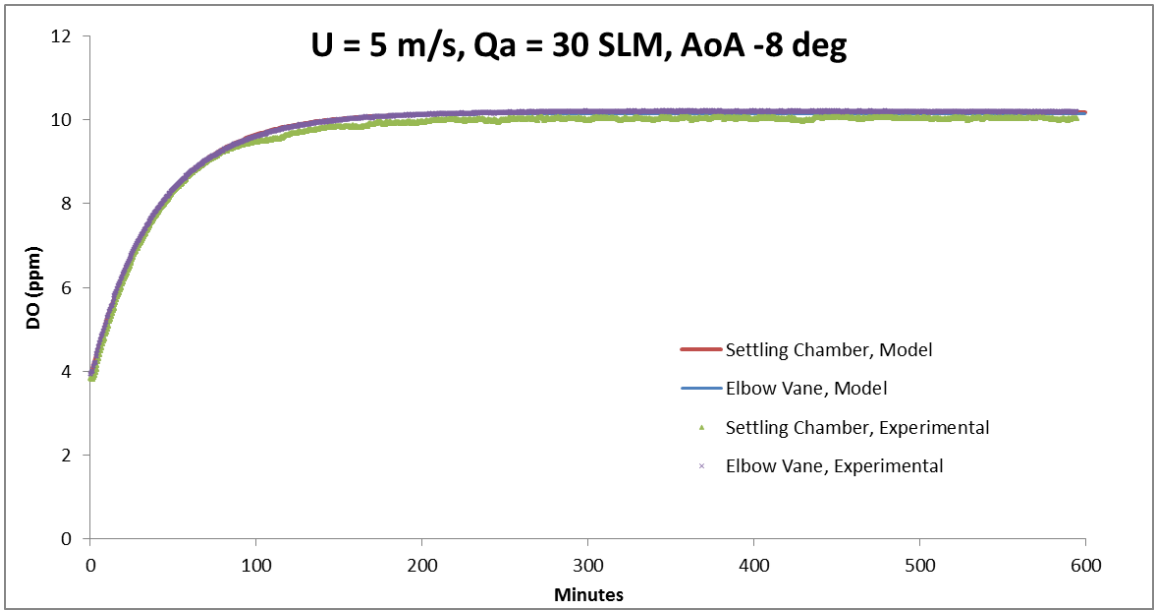
U = 5 m/s, Qa = 30 SLM, AoA -8 deg
DO (ppm)
Minutes
0
2
4
6
8
10
12
0
100
200
300
400
500
600
Settling Chamber, Model
Elbow Vane, Model
Settling Chamber, Experimental
Elbow Vane, Experimental

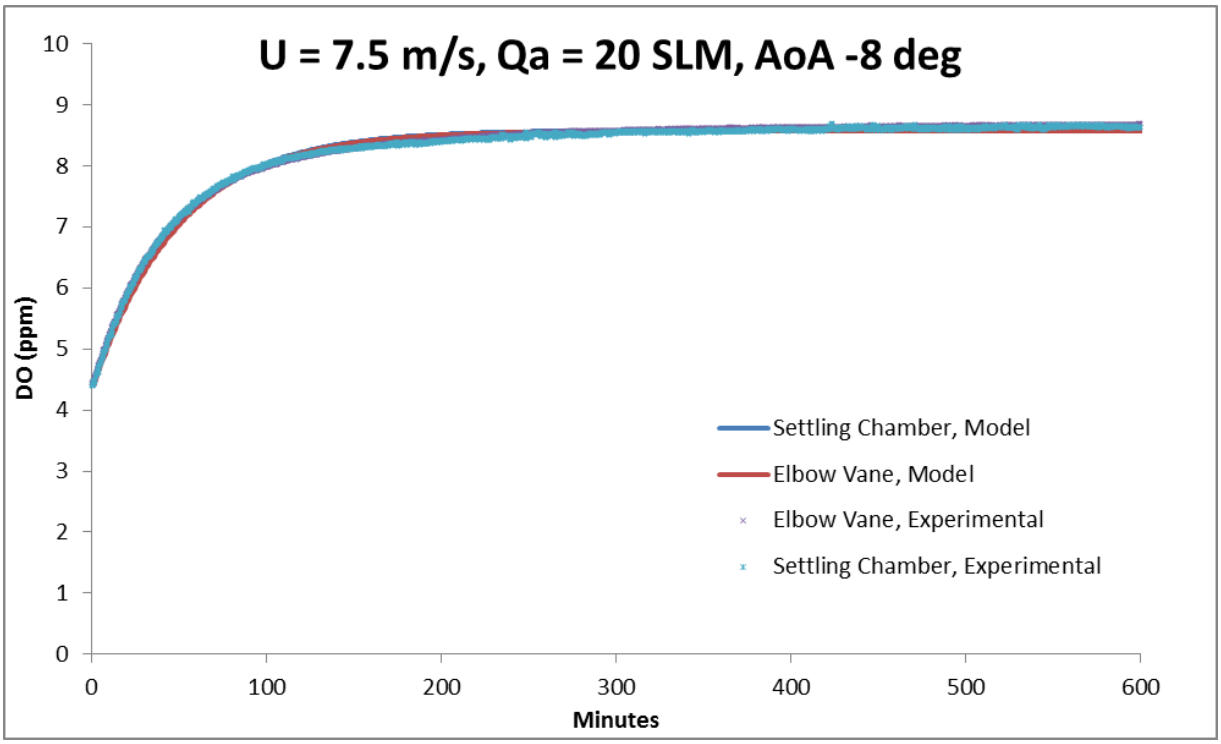
U = 7.5 m/s, Qa = 20 SLM, AoA -8 deg
DO (ppm)
Minutes
0
1
2
3
4
5
6
7
8
9
10
0
100
200
300
400
500
600
Settling Chamber, Model
Elbow Vane, Model
Elbow Vane, Experimental
Settling Chamber, Experimental

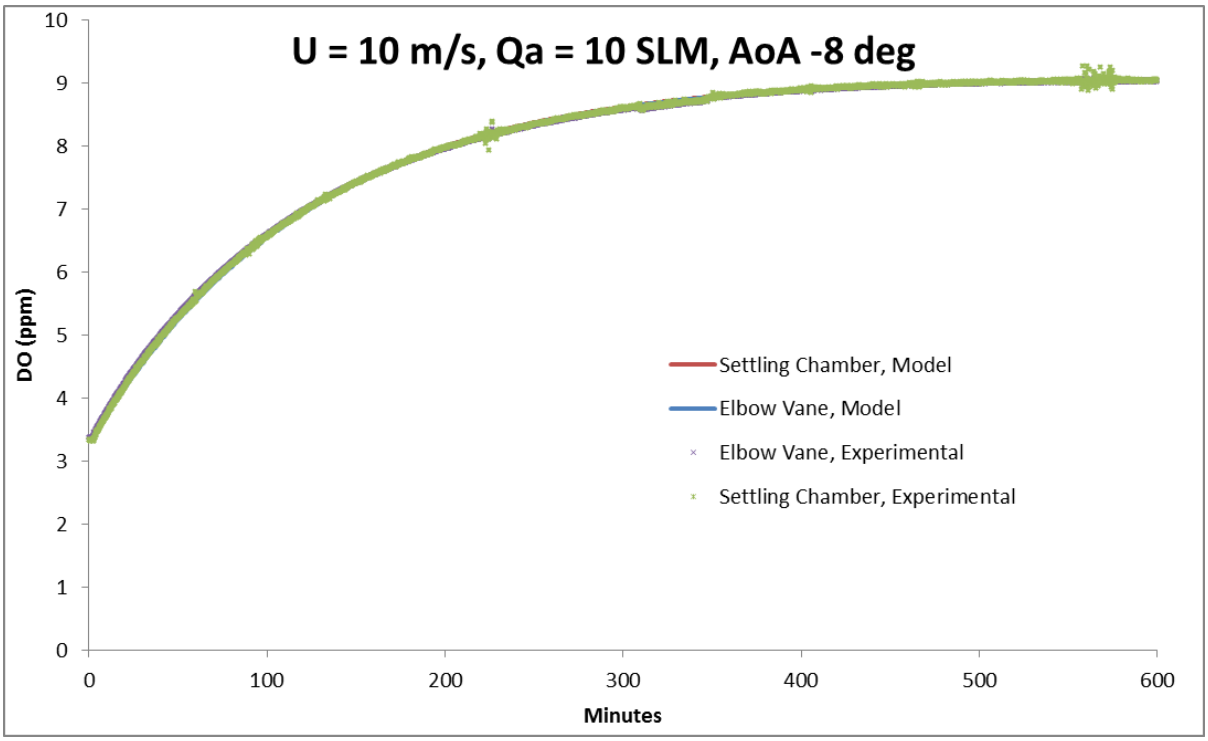
U = 10 m/s, Qa = 10 SLM, AoA -8 deg
DO (ppm)
Minutes
0
1
2
3
4
5
6
7
8
9
10
0
100
200
300
400
500
600
Settling Chamber, Model
Elbow Vane, Model
Elbow Vane, Experimental
Settling Chamber, Experimental

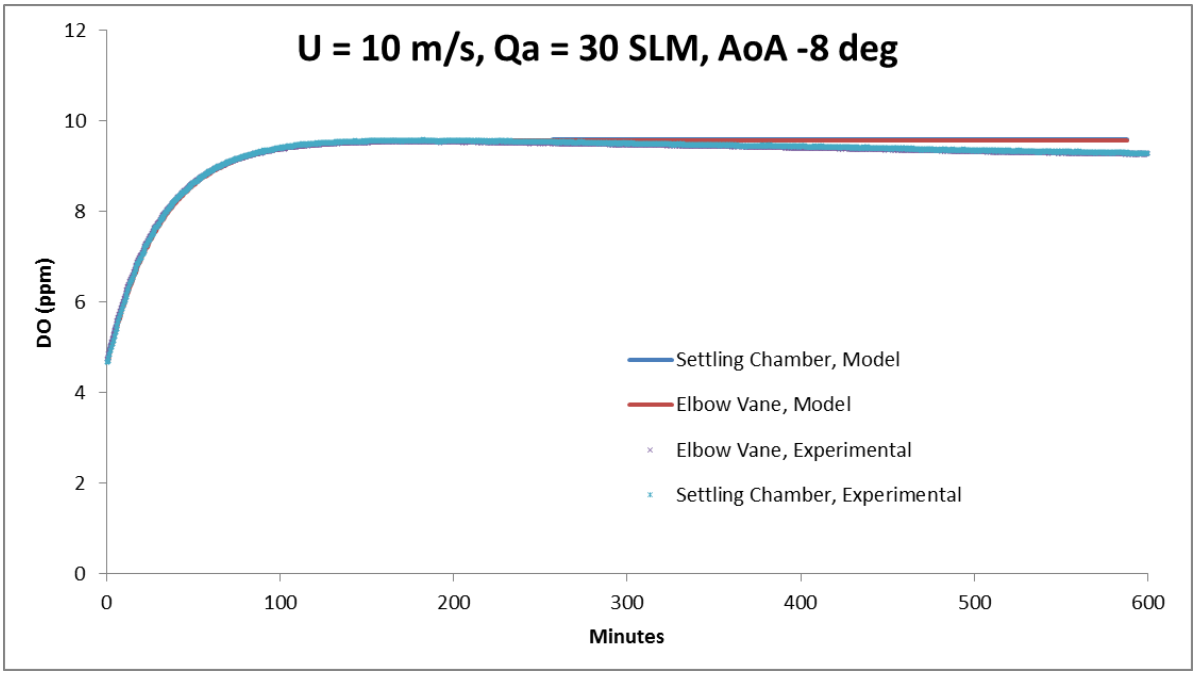
U = 10 m/s, Qa = 30 SLM, AoA -8 deg
DO (ppm)
Minutes
0
2
4
6
8
10
12
0
100
200
300
400
500
600
Settling Chamber, Model
Elbow Vane, Model
Elbow Vane, Experimental
Settling Chamber, Experimental

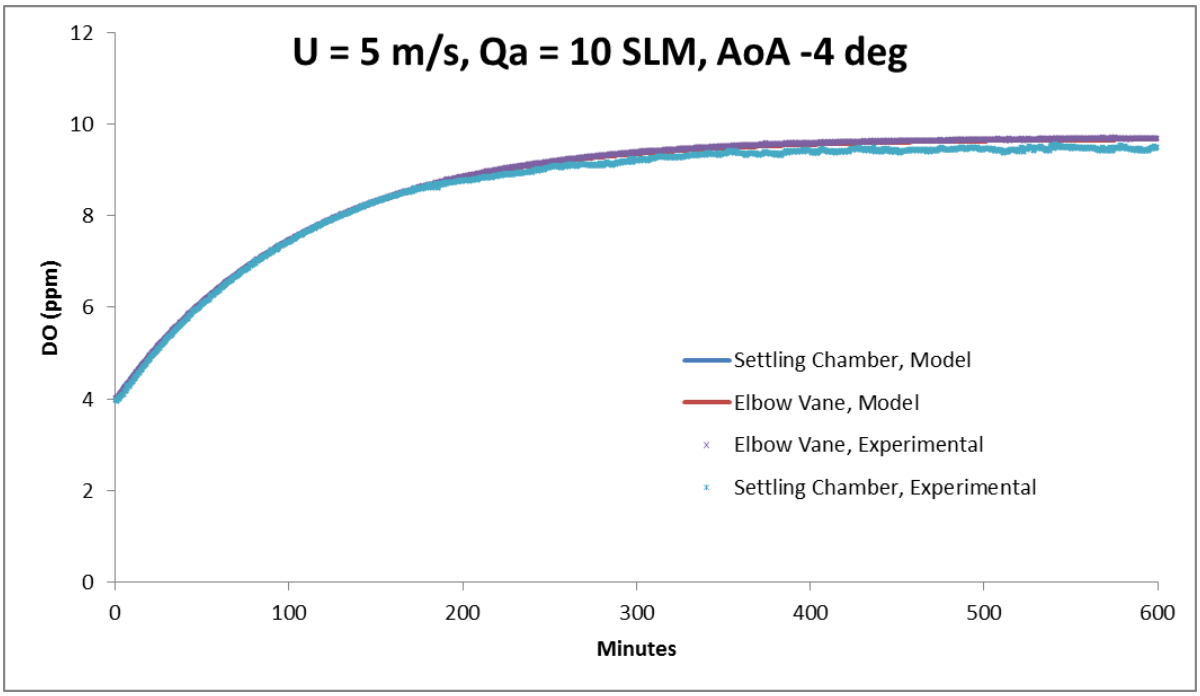
U = 5 m/s, Qa = 10 SLM, AoA -4 deg
DO (ppm)
Minutes
0
2
4
6
8
10
12
0
100
200
300
400
500
600
Settling Chamber, Model
Elbow Vane, Model
Elbow Vane, Experimental
Settling Chamber, Experimental

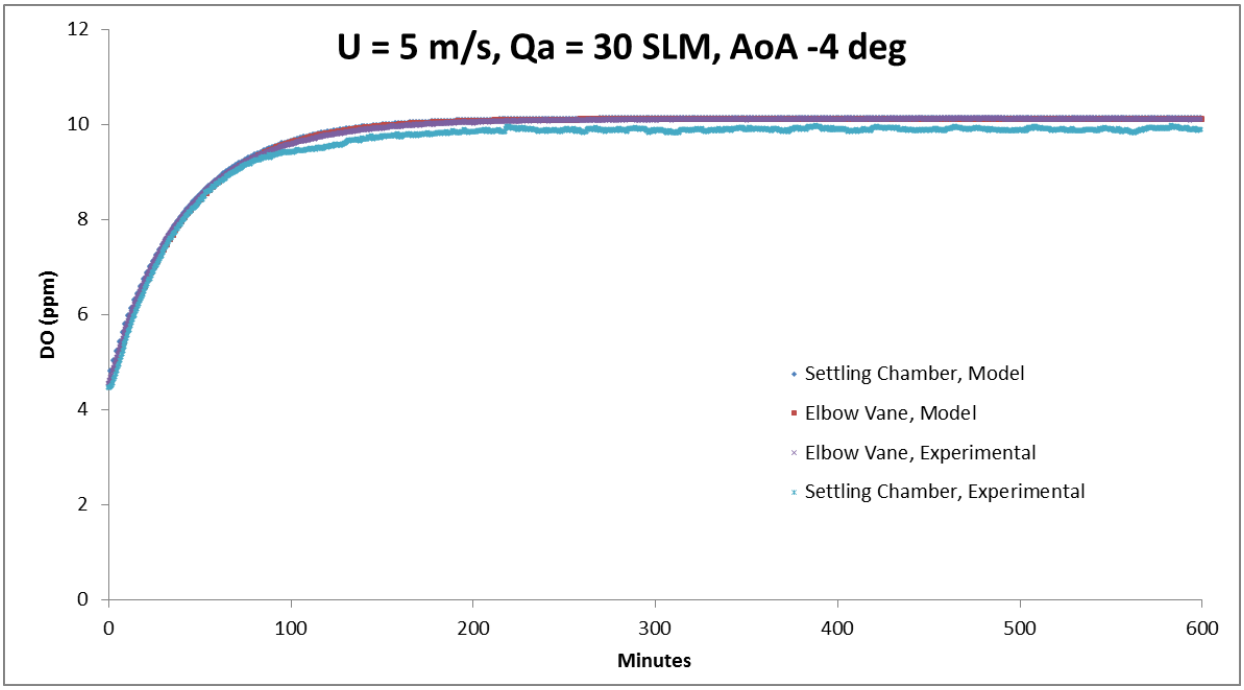
U = 5 m/s, Qa = 30 SLM, AoA -4 deg
DO (ppm)
Minutes
0
2
4
6
8
10
12
0
100
200
300
400
500
600
Settling Chamber, Model
Elbow Vane, Model
Elbow Vane, Experimental
Settling Chamber, Experimental

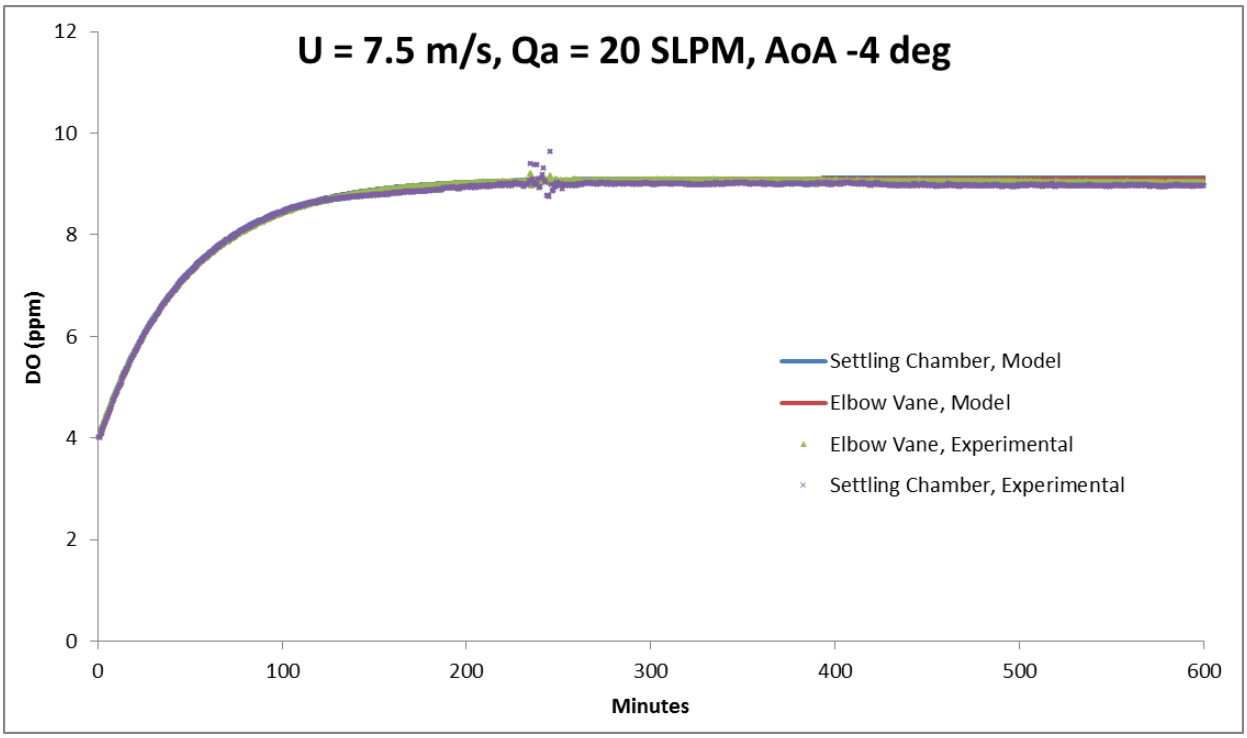
U = 7.5 m/s, Qa = 20 SLPM, AoA -4 deg
DO (ppm)
Minutes
0
2
4
6
8
10
12
0
100
200
300
400
500
600
Settling Chamber, Model
Elbow Vane, Model
Elbow Vane, Experimental
Settling Chamber, Experimental

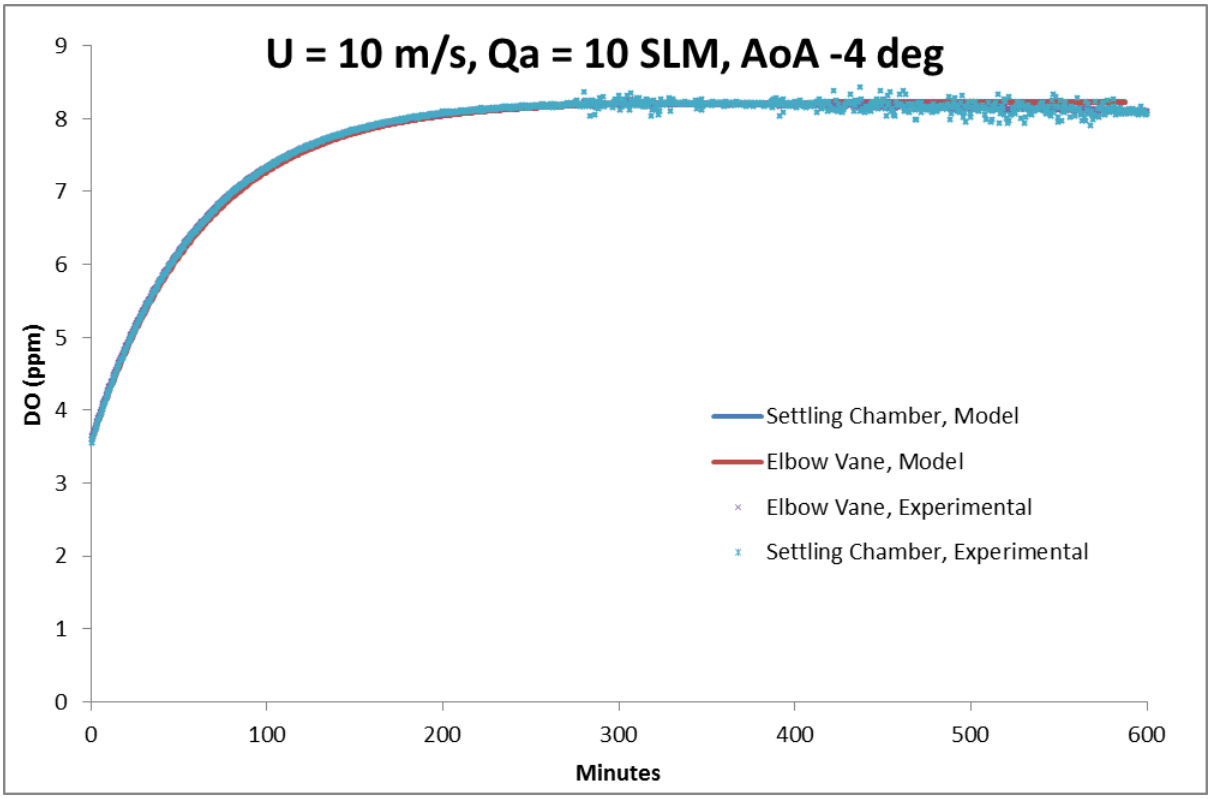
U = 10 m/s, Qa = 10 SLM, AoA -4 deg
DO (ppm)
Minutes
0
1
2
3
4
5
6
7
8
9
0
100
200
300
400
500
600
Settling Chamber, Model
Elbow Vane, Model
Elbow Vane, Experimental
Settling Chamber, Experimental

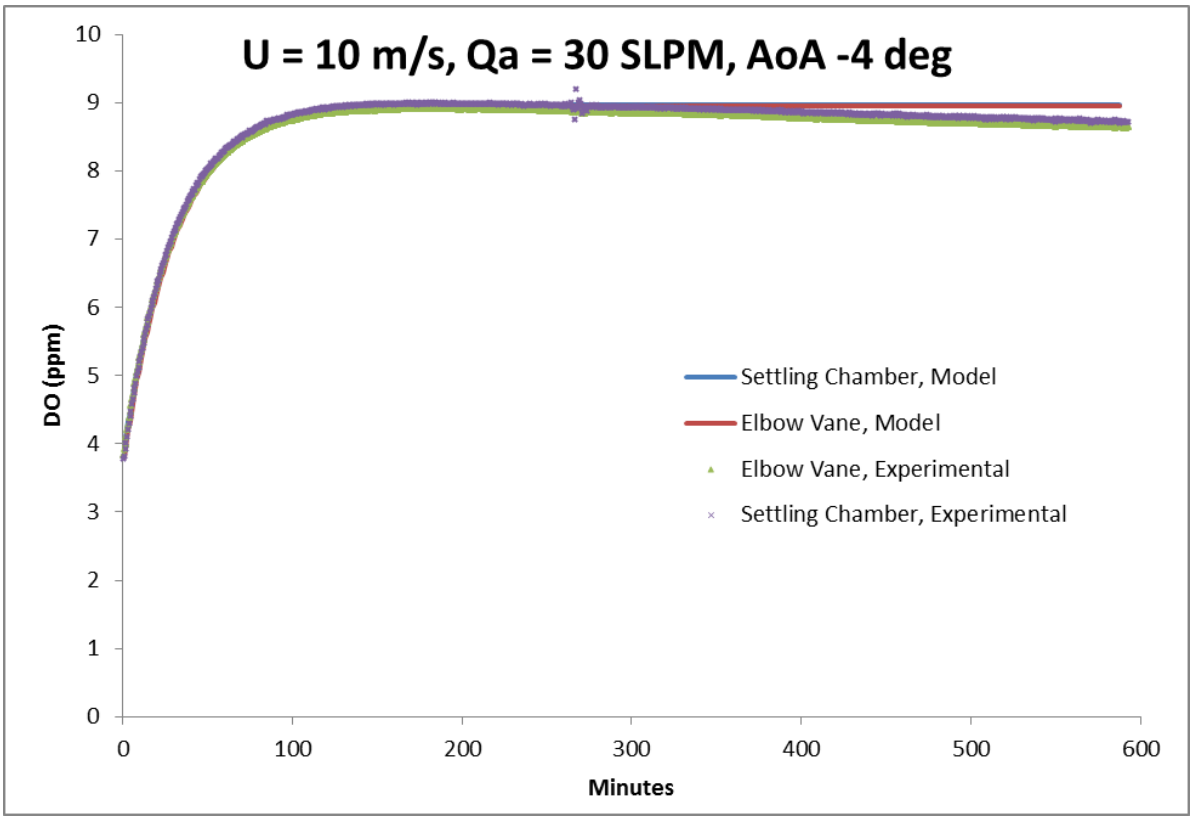
U = 10 m/s, Qa = 30 SLPM, AoA -4 deg
DO (ppm)
Minutes
0
1
2
3
4
5
6
7
8
9
10
0
100
200
300
400
500
600
Settling Chamber, Model
Elbow Vane, Model
Elbow Vane, Experimental
Settling Chamber, Experimental

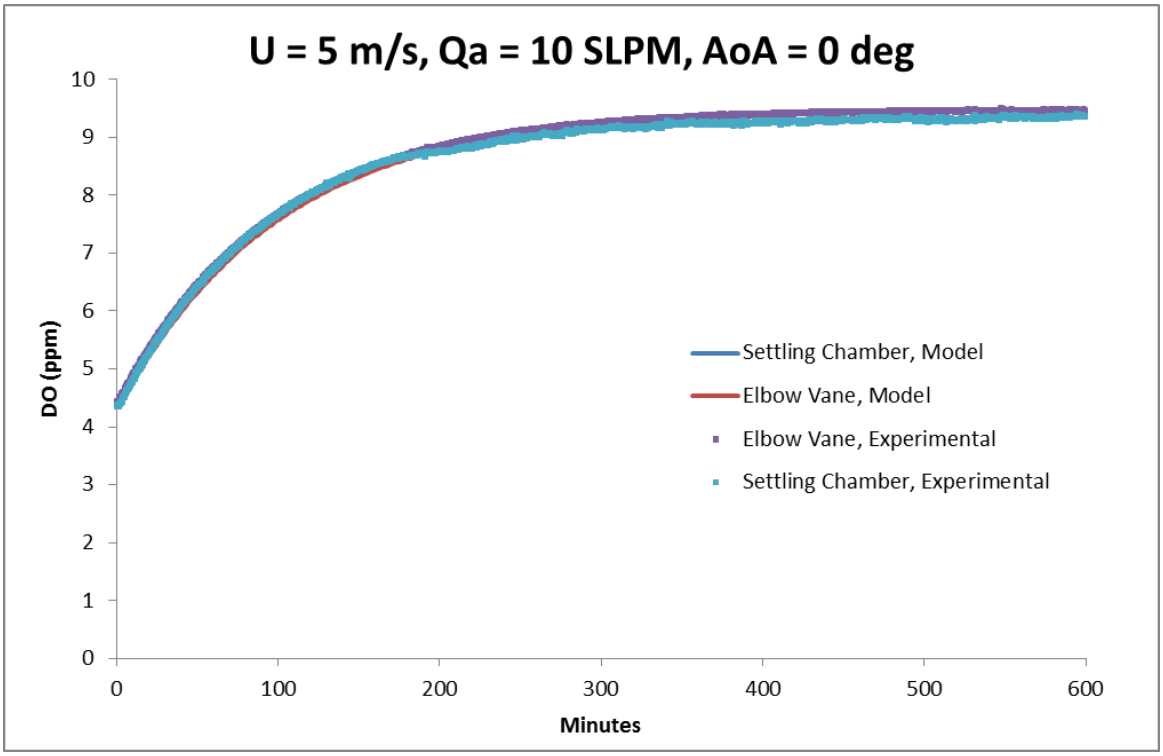
U = 5 m/s, Qa = 10 SLPM, AoA = 0 deg
DO (ppm)
Minutes
0
1
2
3
4
5
6
7
8
9
10
0
100
200
300
400
500
600
Settling Chamber, Model
Elbow Vane, Model
Elbow Vane, Experimental
Settling Chamber, Experimental

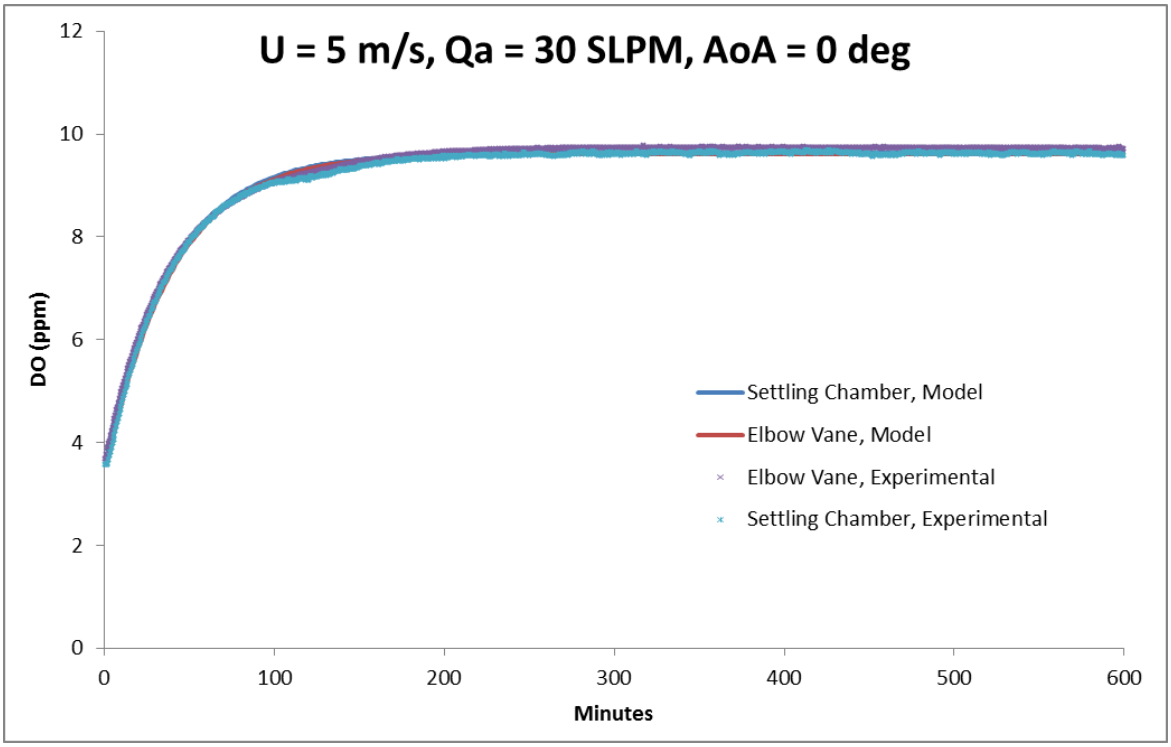
U = 5 m/s, Qa = 30 SLPM, AoA = 0 deg
DO (ppm)
Minutes
0
2
4
6
8
10
12
0
100
200
300
400
500
600
Settling Chamber, Model
Elbow Vane, Model
Elbow Vane, Experimental
Settling Chamber, Experimental

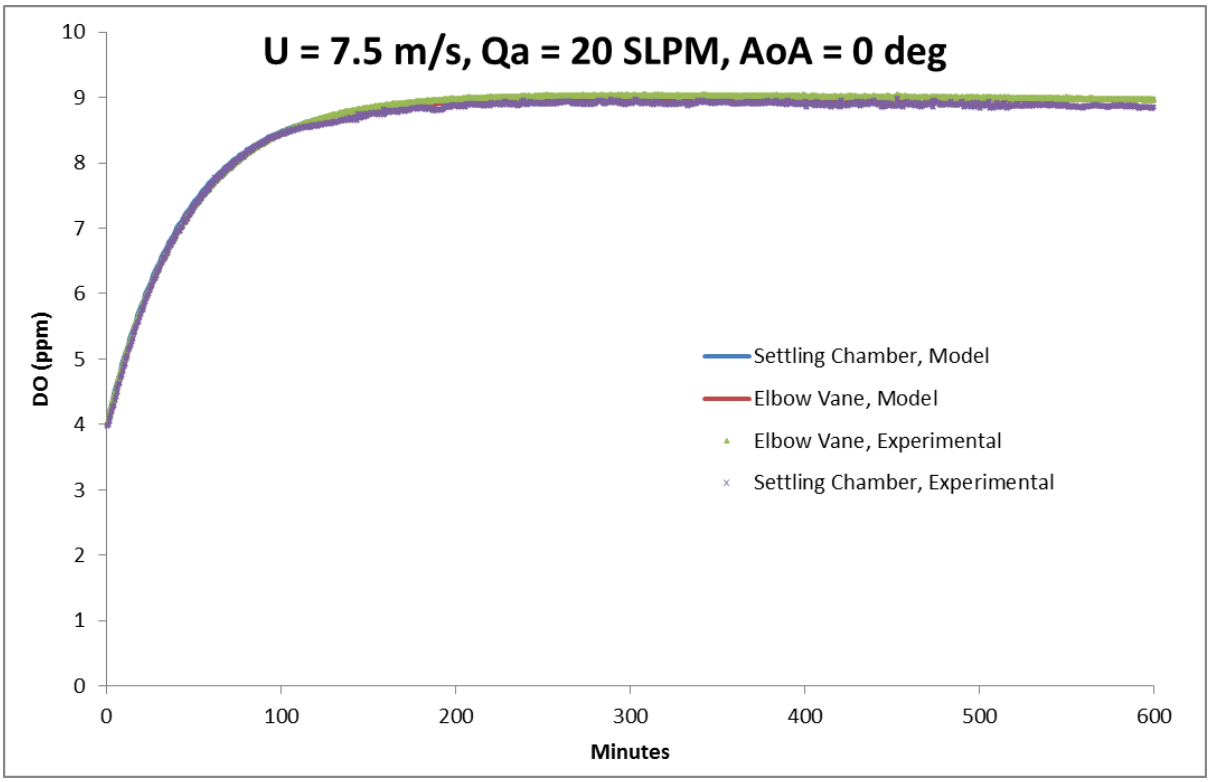
U = 7.5 m/s, Qa = 20 SLPM, AoA = 0 deg
DO (ppm)
Minutes
Settling Chamber, Model
Elbow Vane, Model
Elbow Vane, Experimental
Settling Chamber, Experimental

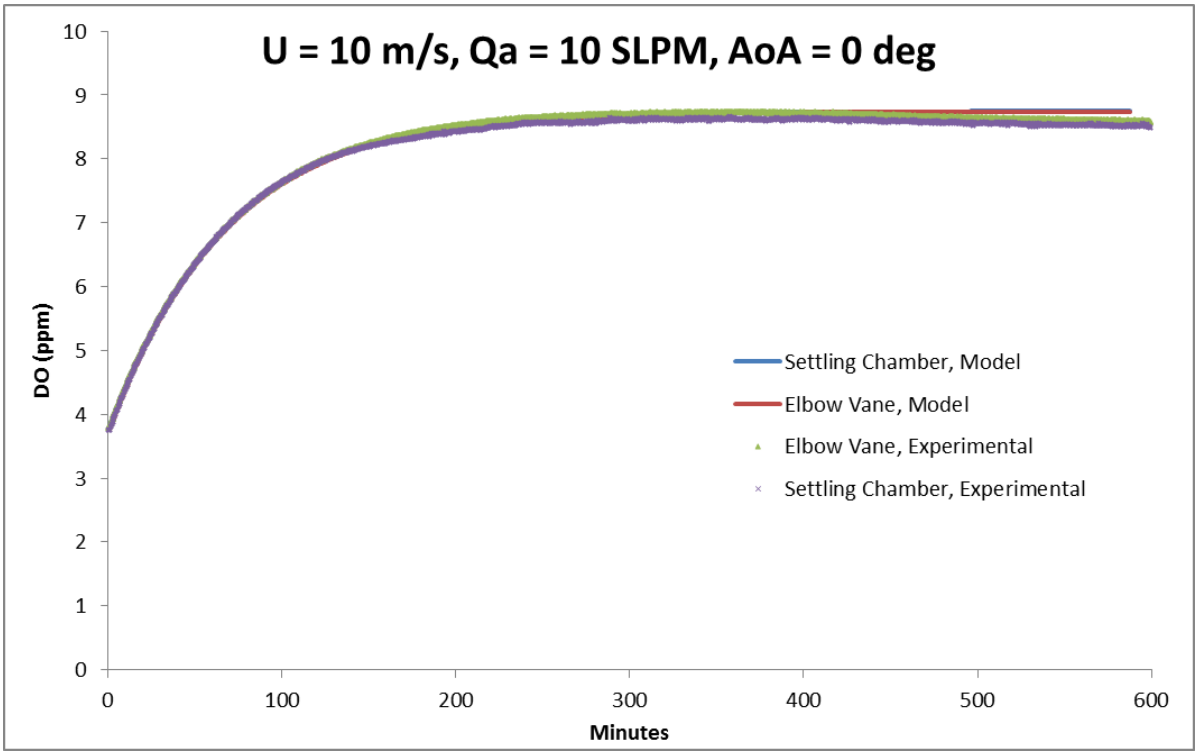
U = 10 m/s, Qa = 10 SLPM, AoA = 0 deg
DO (ppm)
Minutes
Settling Chamber, Model
Elbow Vane, Model
Elbow Vane, Experimental
Settling Chamber, Experimental

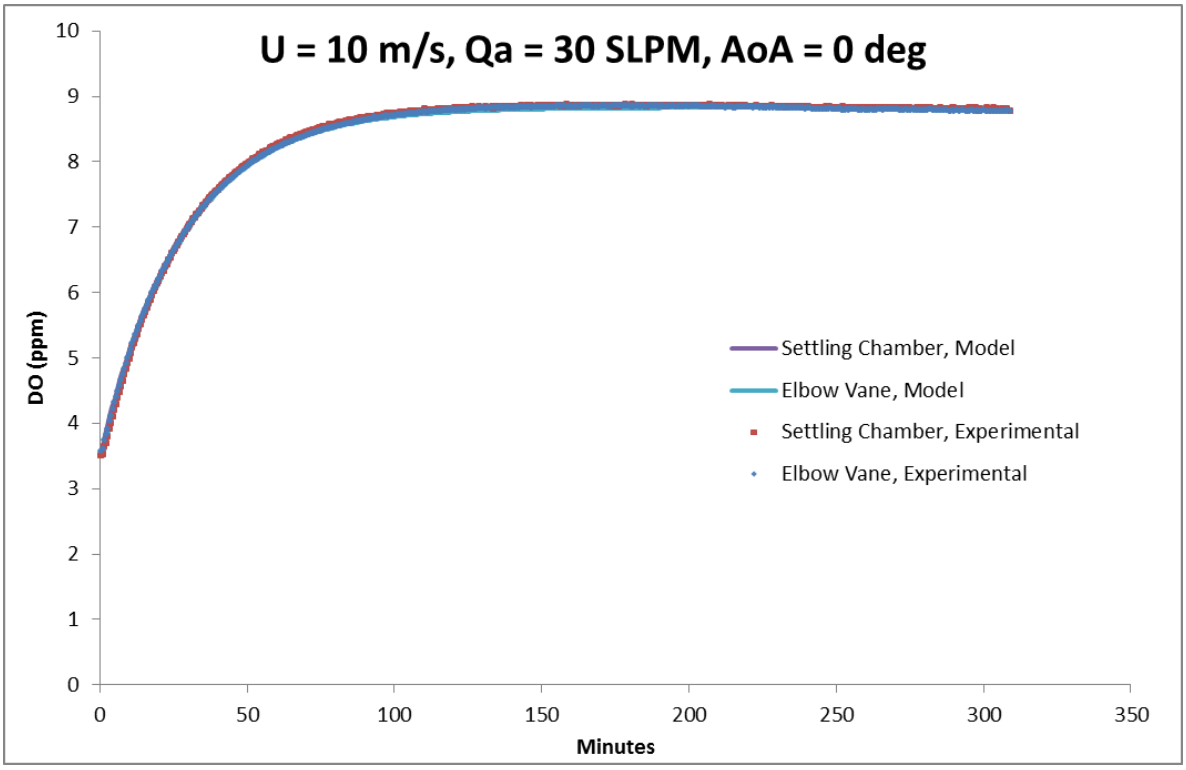
U = 10 m/s, Qa = 30 SLPM, AoA = 0 deg
DO (ppm)
Minutes
0
1
2
3
4
5
6
7
8
9
10
0
50
100
150
200
250
300
350
Settling Chamber, Model
Elbow Vane, Model
Settling Chamber, Experimental
Elbow Vane, Experimental

Appendix B: Uncertainty in Velocity

Velocity in the tunnel is found using a differential pressure transducer (Validyne DP15-50). It measures the pressure difference between the upstream settling chamber and the test section. Velocity is obtained by using the Bernoulli equation for steady incompressible flow.

Bernoulli: $$P_{sc}+\frac{1}{2}\rho U_{sc}^2 = P_{ts}+\frac{1}{2}\rho U_{ts}^2$$

The nozzle contraction ratio is ~39:1. An assumption is made that the velocity of the fluid in the settling chamber, at the point of measurement, is zero. Rearranging the Bernoulli equation, the velocity is computed by

$$U_{ts} = \sqrt{\frac{2(P_{sc}-P_{ts})}{\rho}}$$

The differential pressure transducer is calibrated off of the mercury manometer located on the pillar near the tunnel. Sample calibration curve is shown below.

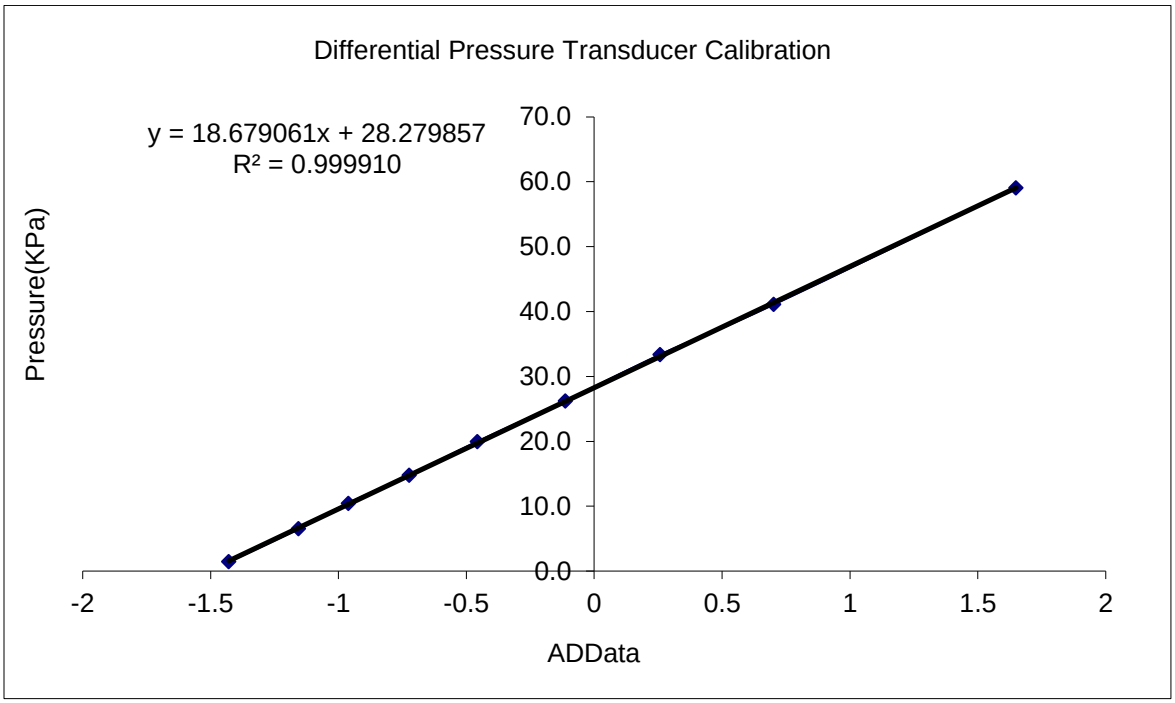

Figure 22. Sample calibration curve for differential pressure transducer

The standard error associated with the linear regression is computed according to the equation

$$\text{Standard Error}=\sqrt{\frac{1}{n-2}\left[\sum(y-\bar{y})^2-\frac{[\sum(x-\bar{x})(y-\bar{y})]^2}{\sum(x-\bar{x})^2}\right]}$$

Once the uncertainty associated with the linear regression is determined, uncertainty in the velocity needs to be determined using uncertainty propagation according to

$$\sigma_b=\left[\sum_{i=1}^{n}\left(\sigma_{xi}\frac{\partial U}{\partial x_i}\right)^2\right]^{1/2}$$

$$\frac{\partial U_{ts}}{\partial \Delta p}=\left(\frac{2\Delta p}{\rho}\right)^{-1/2};\frac{\partial U_{ts}}{\partial \Delta p}=-\frac{\sqrt{2\Delta p}}{2\rho^{3/2}}$$

Assuming the uncertainty in the density is negligible, the uncertainty in velocity simplifies to

$$\sigma_b=\sigma_{\Delta p}\frac{\partial U_{ts}}{\partial \Delta p}=\sigma_{\Delta p}\left(\frac{2\Delta p}{\rho}\right)^{-1/2}$$

Example:

Table 7. Data used to generate calibration curve.

transducer reading (counts)	dp (kPa)	U (m/s)	s_U (m/s)	%Uncertainty
-1.42843	1.477	1.7202	0.108	6.299367615
-1.15582	6.523	3.61515	0.052	1.426271913
-0.96085	10.461	4.578233	0.041	0.889322487
-0.722553	14.769	5.439751	0.034	0.629936762
-0.457098	19.938	6.32042	0.029	0.466619823
-0.112209	26.215	7.247333	0.026	0.35489395
0.25833	33.353	8.174723	0.023	0.278938787
0.70208	41.107	9.075314	0.021	0.226324585
1.64937	59.075	10.8795	0.017	0.15748419
Standard Error =	0.1864039	kPa		

Appendix C: Degassing Loop Operation

Degassing Loop Operation

Start up:

1. Close both valves above the test section and the main valve to atmosphere



2. Run the water tunnel at a very low speed (5 Hz, ~70 RPM)

3. Open 3” drain valve under settling chamber

4. Turn on degassing loop pump under stairs

5. Open return leg 3” valve mounted under settling chamber

Initiating Vacuum

1. Close all valves on free jet tunnel excluding the vacuum line valve
2. Leave vacuum valve open

3. Close all valves on the free jet control panel

4. Ensure the discharge valve is at ~2.75 inches
5. Open free jet main valve gradually by jacking the manual hydraulic lever

6. Open the main valve until the flow through the test section is solid

7. There should be a vacuum pressure indicated on the degassing chamber

8. Adjust flow through free jet with manual hydraulic lever and control valve as needed

Stopping Vacuum

1. Open all ventilation valves on the Free Jet Tunnel
2. Gradually open the intake control panel valve all the way
3. Flow through the free jet tunnel should stop, except minor flows due to leaks

Shutting down loop

1. Turn off the pump beneath the stairs
2. Close the return leg 3” valve
3. Close the 3” drain valve under settling chamber
4. Open water tunnel atmospheric valve
5. Stop water tunnel

Appendix D: Calibration of Pressure Transducers

The pressure transducers that measured the static pressure in the water tunnel test section, P_∞, the pressure inside the elbow vane, P_{EV}, and the differential pressure, $P0 - P_\infty$, were calibrated with each change in angle of attack and before each series of experiments. The calibrations were performed using two mercury manometers, one for each transducer. Before calibration, the pressure lines were purged to ensure no air bubbles were trapped in them.

When calibrating the absolute pressure transducer that measured P_∞, one leg of the manometer was connected to the static pressure port while the other leg was connected to a tank filled with water whose level was at the same height as the static port in the water tunnel test section. The pressure in the tunnel was then varied by pulling a vacuum in the water tunnel. At each calibration point, the height of the mercury column and the pressure transducer output were recorded. Approximately 10 calibration points were taken each time the transducer was calibrated. After calibration, the pressure in the tunnel was relieved to atmospheric pressure.

After calibrating the test section absolute pressure transducer, the elbow pressure absolute pressure transducer was calibrated. A vacuum was then pulled in the test section and the elbow vane pressure transducer was calibrated using the test section absolute pressure transducer.

After calibrating the absolute pressure transducers, the differential pressure transducer was calibrated. When calibrating the differential pressure transducer, one leg of the manometer was connected to the stagnation pressure in the settling chamber of the test section while the other leg was connected to the static port in the test section. The differential pressure in the tunnel was then varied by changing the free stream velocity.

Again, at each calibration point the height of the mercury column and the pressure transducer output were recorded. After calibrating the three pressure transducers, the calibration curves were created by plotting the differential pressure given by the manometers versus transducer output. A straight line was then fit through the data for each transducer using least squares fit. The pressure transducer calibrations produced curves that were consistently linear,

with R-squared values typically 0.9999 or higher for both the all transducers. Errors due to the least squares fit line were approximately 0.1 kPa for both absolute pressure transducers. These errors lead to a maximum error in the measured velocity of 0.11 m/s,
with typical errors being closer to 0.02 m/s.